Form Approved
Budget Bureau No. 22-R0293

FINAL REPORT

February 1978

to

Air Force Office of Scientific Research

from

Department of Geological Sciences
Cornell University
Ithaca, New York 14853

Title of Proposal:	Contemporary Tectonics of China
Report Prepared by:	James Ni
Sponsored by:	Advanced Research Projects Agency ARPA Order No. 3291
Program Code:	7F10
Effective Date of Contract:	1 October 1976
Contract Expiration Date:	30 September 1977
Amount of Contract Dollars:	$30,000
Contract Number:	AFOSR 77-3170
Program Manager:	William J. Best 202-693-0162
Principal Investigator:	Jack E. Oliver 607-256-2377 Bryan L. Isacks 607-256-2307

Jack E. Oliver, Principal Investigator

Bryan L. Isacks, Principal Investigator

Sponsored by
Advanced Research Projects Agency (DOD)
ARPA Order No. 3291
Monitored by AFOSR Under Grant #AFOSR 77-3170

UNCLASSIFIED

SECURITY CLASSIFICATION OF THIS PAGE *(When Data Entered)*

REPORT DOCUMENTATION PAGE		READ INSTRUCTIONS BEFORE COMPLETING FORM
1. REPORT NUMBER	2. GOVT ACCESSION NO. AD-A131 742	3. RECIPIENT'S CATALOG NUMBER
4. TITLE *(and Subtitle)* Contemporary Tectonics of China		5. TYPE OF REPORT & PERIOD COVERED FINAL REPORT 10 Oct 1976 - 30 Sept. 1977
		6. PERFORMING ORG. REPORT NUMBER
7. AUTHOR(s) James Ni		8. CONTRACT OR GRANT NUMBER(s) AFOSR 77-3170
9. PERFORMING ORGANIZATION NAME AND ADDRESS Department of Geological Sciences Cornell University Ithaca, New York 14853		10. PROGRAM ELEMENT, PROJECT, TASK AREA & WORK UNIT NUMBERS Project Task AO 3291-1
11. CONTROLLING OFFICE NAME AND ADDRESS Air Force Office of Scientific Research 1400 Wilson Blvd. Arlington, Virginia 22209		12. REPORT DATE February 1978
		13. NUMBER OF PAGES 10 pages plus 2 appendices
14. MONITORING AGENCY NAME & ADDRESS(if different from Controlling Office) Same		15. SECURITY CLASS. (of this report) Unclassified
		15a. DECLASSIFICATION/DOWNGRADING SCHEDULE

16. DISTRIBUTION STATEMENT *(of this Report)*

Approved for public release; distribution unlimited.

17. DISTRIBUTION STATEMENT *(of the abstract entered in Block 20, if different from Report)*

18. SUPPLEMENTARY NOTES

None

19. KEY WORDS *(Continue on reverse side if necessary and identify by block number)*

Tectonics, LANDSAT imagery, faulting, focal mechanism solution, China.

20. ABSTRACT *(Continue on reverse side if necessary and identify by block number)*

Seismic data and LANDSAT imagery in western China have been investigated in detail. Fault plane solutions of earthquakes that occurred in the past ten years were derived from polarities of first motions of P and S waves. Numerous faults and fault systems were identified from LANDSAT imageries. In particular, a new strike-slip fault (the Po Chu fault) and numerous normal faults in the Tibetan Plateau were discovered. The type and sense of faulting were deduced from adjacent geomorphic features seen on these imagery, from fault plane solutions of earthquakes, and from field reports. Analysis has shown positive correlations

DD FORM 1 JAN 73 1473 EDITION OF 1 NOV 65 IS OBSOLETE

Unclassified

SECURITY CLASSIFICATION OF THIS PAGE *(When Data Entered)*

20. between epicenters of strong earthquakes and major faults in the southern Tien Shan and the Tibetan regions.

ABSTRACT

Seismic data and LANDSAT imagery in western China have been investigated in detail. Fault plane solutions of earthquakes that occurred in the past ten years were derived from polarities of first motions of P waves and S waves. Numerous faults and fault systems were identified from LANDSAT imageries. In particular, a new strike-slip fault (the Po Chu fault) and numerous normal faults in the Tibetan Plateau were discovered. Lineaments on the imagery were interpreted as late Cenozoic faults primarily primarily based on linearity, sharpness of a scarp, and presence of a topographic, tonal or textural difference across the lineament. Characteristics of different types of faulting can be inferred from their geomorphology. Normal faults are indicated by sharp, broken, and en echelon fault traces. Major strike-slip faults are characterized by long linear traces. Evidence for recent motions along such faults is provided by sharp offsets in the Quaternary alluvium, ponding of streams, and offset of streams. Analysis has shown positive correlations between epicenters of strong earthquakes and major faults in the southern Tien Shan and Tibetan regions.

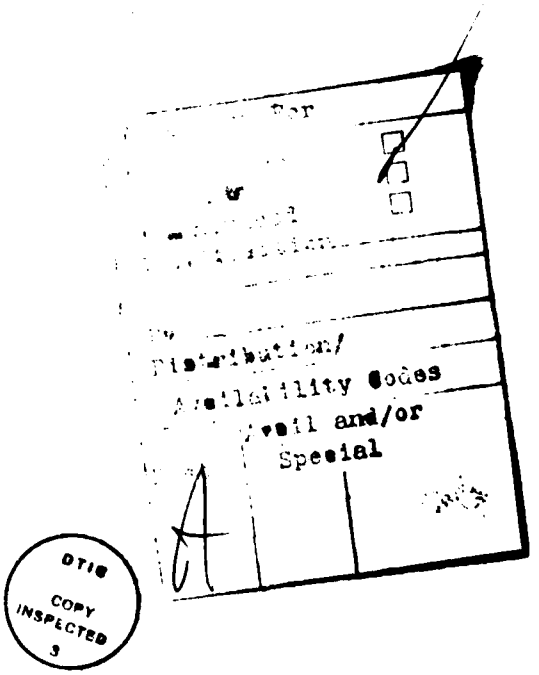

Technical Problem

Although a successful theoretical and empirical framework has been developed for understanding seismicity near lithospheric plate boundaries, earthquakes occurring within these boundaries remain an enigma. Intraplate earthquakes are less common than seismic events in active tectonic regions, but they are known to reach large magnitudes. In general, we do not understand why or how such shocks occur, what geological features they are associated with, where they may be expected to occur in the future, or why their seismograms in many ways more closely resemble those of buried nuclear explosions than those of shocks in the major seismic belts. An increased understanding of intraplate earthquakes is essential in the planning of major constructions such as dams, nuclear power plants and other large structures. It is also necessary for the safety of thousands or even millions of lives. The recent successes in earthquake prediction by the Chinese indicate that it would be of value to the United States to understand seismicity in China because their methods used in predicting large intraplate seismic events can be applied to predicting large seismic events in the United States. An increased understanding of intraplate earthquakes can also improve our ability to discriminate between natural events and nuclear explosions.

General Method

In order to circumvent the limitations placed on studies of Chinese seismicity by the infrequent occurrence of intraplate earthquakes, data from instrumentally, located epicenters, fault plane solutions, and geologic evidence for long-term movements were incorporated and evaluated in this study. Literature reviews on Tibet and Tien Shan regions have been completed. LANDSAT data is of great value in studying the tectonics of China because ground observations by western scientists are not possible. The imagery has revealed previously unknown, large, strike-slip faults in China. Ponding of streams and offset of alluvium on these and other faults are evidence that the faults are active. The mapping of geologic features has been integrated with fault plane solutions, seismicity patterns, and regional stress patterns.

Earthquake swarms and aftershock sequences were also studied with the Joint Hypocenter Determination (JHD) technique to yield very accurate relative locations. Fault planes may be determined with this method, thereby removing the ambiguity of the choice of fault plane from a fault plane solution. Data from the World Wide Network of Seismograph Stations (WWNSS) were used for the JHD method. First P motions from long-period seismograms and S-wave polarizations were used to

construct fault plane solutions. These fault plane solutions and the previously determined ones have improved the understanding of local stress patterns and regional tectonics.

Technical Results

Studies completed during this contract are:

1. A comprehensive study of the Late Cenozoic "Tectonics of the Tibetan Plateau," which has been submitted to the Journal of Geophysical Research for publication, is attached as Appendix 1. In this study, normal faulting interpreted from LANDSAT imagery and fault plane solutions of earthquakes suggest late Cenozoic east-west extension in the Tibetan Plateau. Normal faulting contrasts with major thrusting along the southern boundary and major strike-slip faulting near the other boundaries of Tibet. The extension may be related to western Tibet being compressed between thrusting on the south and strike-slip faulting on the northwest and consequently spreading along an east-west trend.

2. A preprint of "Contemporary Tectonics in the Tien Shan Region," which the author is planning to submit to Earth and Planetary Science Letters, is attached as Appendix 2. In this study seismic data show that the principal earthquake zones of the Tien Shan region are clearly related to the neotectonic structures. For most of the fault plane solutions compressive stress axes are nearly horizontal and trending approximately N-S, perpendicular to the trend of the Tien Shan fold belts. The southeastern Tien Shan region is characterized by northward thrusting. In contrast, the southwestern Tien Shan region is characterized by southward thrusting. Between these two major thrust belts the Talaso-Fargana right laterial strike-slip fault appears to be absorbing the differential horizontal shortening.

3. Relocation of the Tien Shan Events with Joint Hypocenter Determination. A series of earthquakes occurred in the eastern Tien Shan during 1969 and 1971 (Figure 1). These earthquakes are mainly of the shock-aftershock sequence type because of the relatively large magnitude of the main shock compared with the magnitude of the aftershocks. The method of Joint Hypocenter Determination (JHD) was used to relocate the epicenters of the earthquakes. The relocations were obtained with this method using a station-corrected calibration event, initial earthquake hypocenters, initial arrival time, and station arrival times of the events, all taken from the Bulletin of the International Seismological

Centre. Thirty earthquakes were relocated by this method with a maximum of 15 possible stations per earthquake and a minimum of 7 stations per earthquake. Stations were chosen to give the best possible uniform azimuthal and epicentral coverage as well as the most reliable readings. Table 1 gives the station epicentral distances and approximate azimuths.

The ISC reported depths less than 47 km for most of these events. These depth determinations are calculated from arrival times of P only. Thus, without pP data or arrival times at stations very close to the source, it is impossible to accurately determine focal depths. Since our primary interest was to develop reliable techniques to determine fault planes from fault plane solutions and satellite imagery, approximation is made by assuming all hypocenters to be at the same depth. The resulting relocated epicenters are shown in Figure 2. The dotted lines represent the approximate trend of aftershocks. This trend is in good agreement with the "A" nodal plane also shown in Figure 2. Therefore, this nodal plane, which strikes N75°W with a shallow north-dipping angle, was chosen for the fault plane.

Interpretation of LANDSAT imagery indicates no obvious lineament trending in this direction. However, the approximately east-west folding in the foothills of the Tien Shan indicates a shallow thrusting dip toward the north. This observation is also in agreement with the general trend of the aftershock sequences. Further study of LANDSAT imagery of different seasons is necessary to determine whether faults can be observed from the imagery.

4. Fault Plane Solution of the Haicheng Earthquake of February 4, 1975. A major earthquake occurred in the Liaoning Province on February 4, 1975. Parameters reported by the U.S.G.S. for this earthquake are: epicenter - 40.641°N, 122.58°E; origin time - 11 h 36 m 7.54 s; depth of focus - normal; magnitude - 7.4 (MS). Data for this earthquake were obtained through WWNSS stations. Only the first motion of P waves and some S-wave polarizations recorded on long-period instruments were used in the construction of the fault plane solution. The mechanism (Figure 3) indicates strike-slip faulting. This earthquake was accompanied by numerous aftershocks. Figure 4 shows the distribution of earthquakes of magnitude 2 and greater between February 1 and May 31, 1975 (Gu et al., 1976). Aftershocks were concentrated in an area 70 km long and 30 km wide, and the epicentral

depth distribution was between 1 and 17 km with most less than 12 km. Therefore, we conclude that the near-vertical east-west trending nodal plane is the fault plane.

Reference

Gu, H. D., Y. T. Chin, X. L. Gao, and Y. Zhao, 1976. Focal mechanism of the Haicheng, Kiaoning Province, earthquake of February 4, 1975, Acta Geologica Sinica, 19, 270-284.

TABLE 1.

Stations Used in the JHD Relocations

Station Abbreviation	Epicentral Distance (deg)	Azimuth (deg)
PRZ	1.19	331
MNL	9.33	209
KBL	10.55	323
NDI	12.83	188
QUE	15.18	226
SHL	18.87	143
GBA	27.69	185
NUR	38.16	319
NIE	41.29	302
KRA	41.31	303
GRF	47.08	304
MBC	62.00	5
COL	67.80	20
YKC	75.84	7
WRA	79.34	129

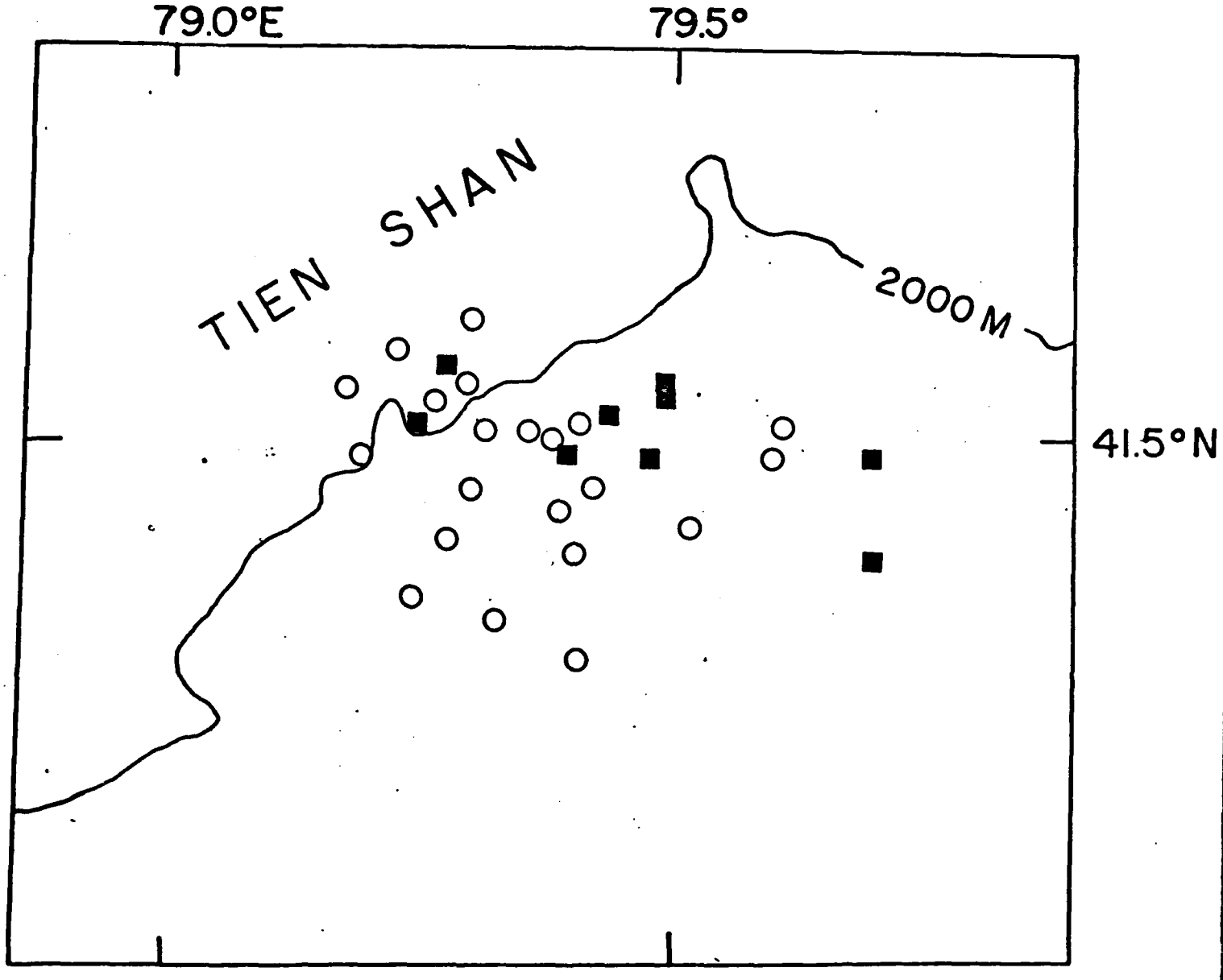

Figure 1. Map shows ISC location of epicenters from 1969 to 1971 events. Solid squares represent 1969 aftershock sequence, open circles represent 1971 aftershock sequence.

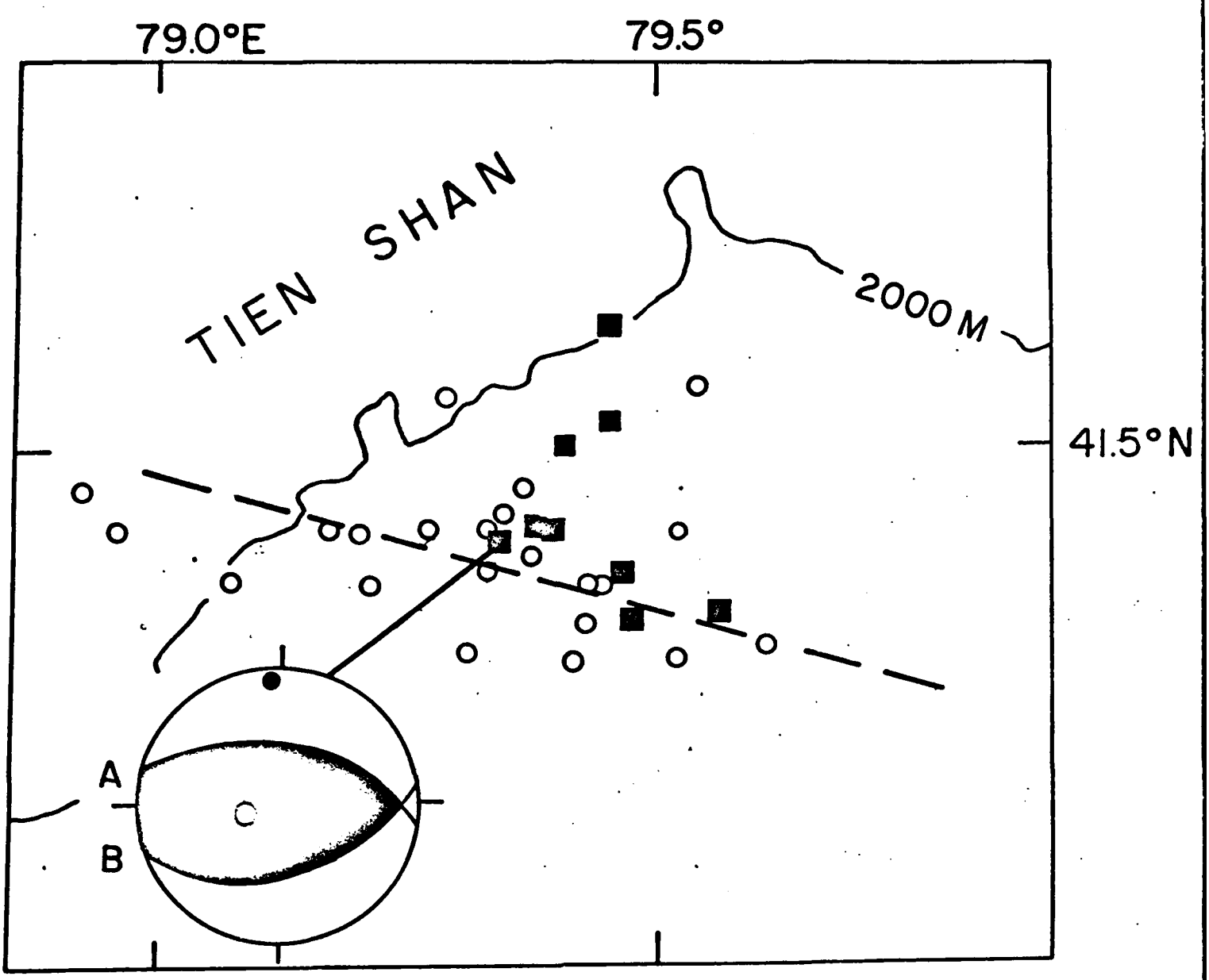

Figure 2. Map shows JHD relocated epicenters from 1969 to 1971 events. Solid squares represent 1969 aftershock sequence, open circles represent 1971 aftershock sequence. Fault plane solution of February 2, 1969 events is taken from Molnar et al., 1973.

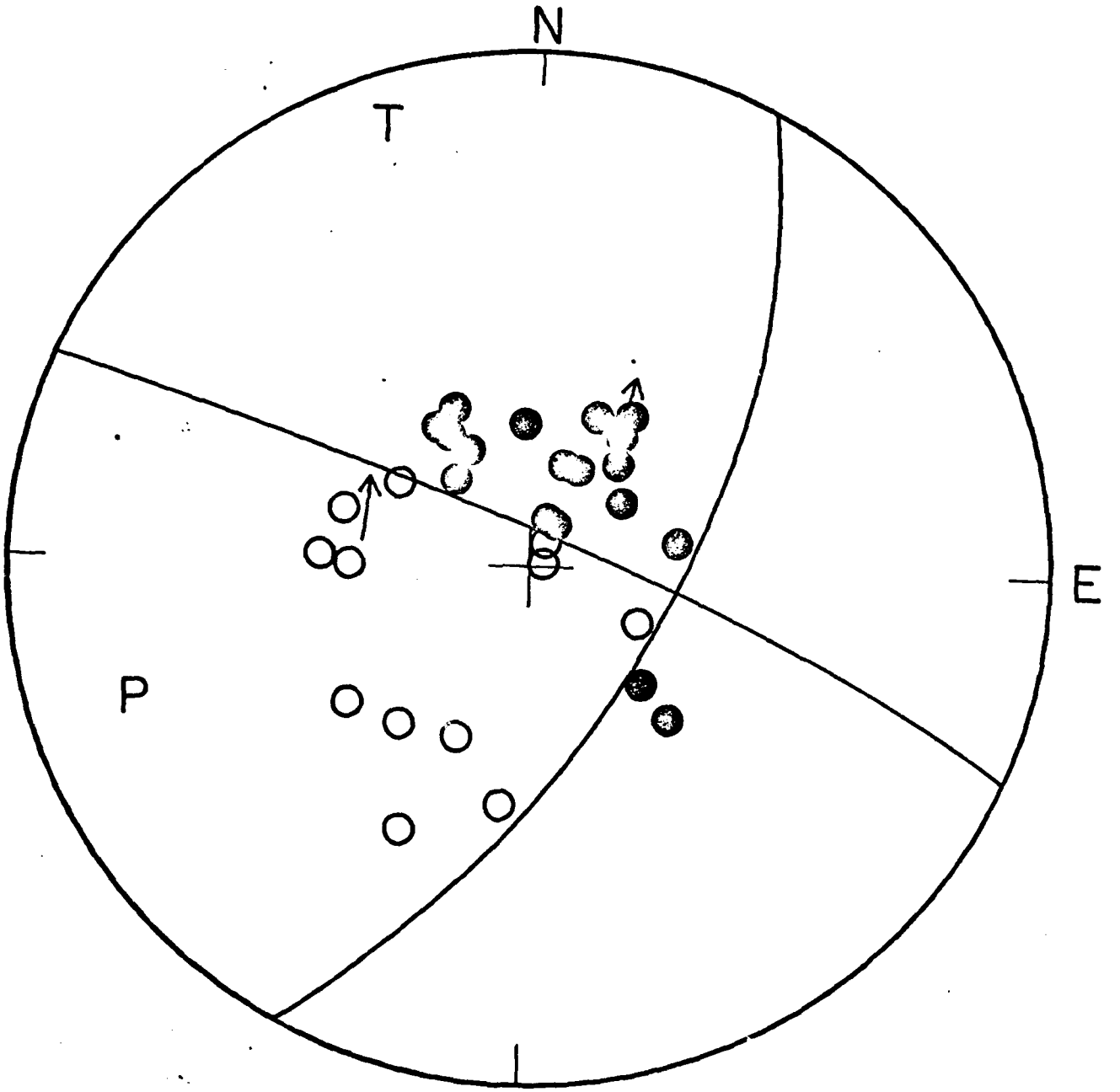

Figure 3. Focal mechanism using lower hemisphere projections. Polarities of P wace first motion are given by solid circles, open circles for dilatation. S-wave polarization is indicated by arrows. P and T are the location of maximum and minimum compression, respectively.

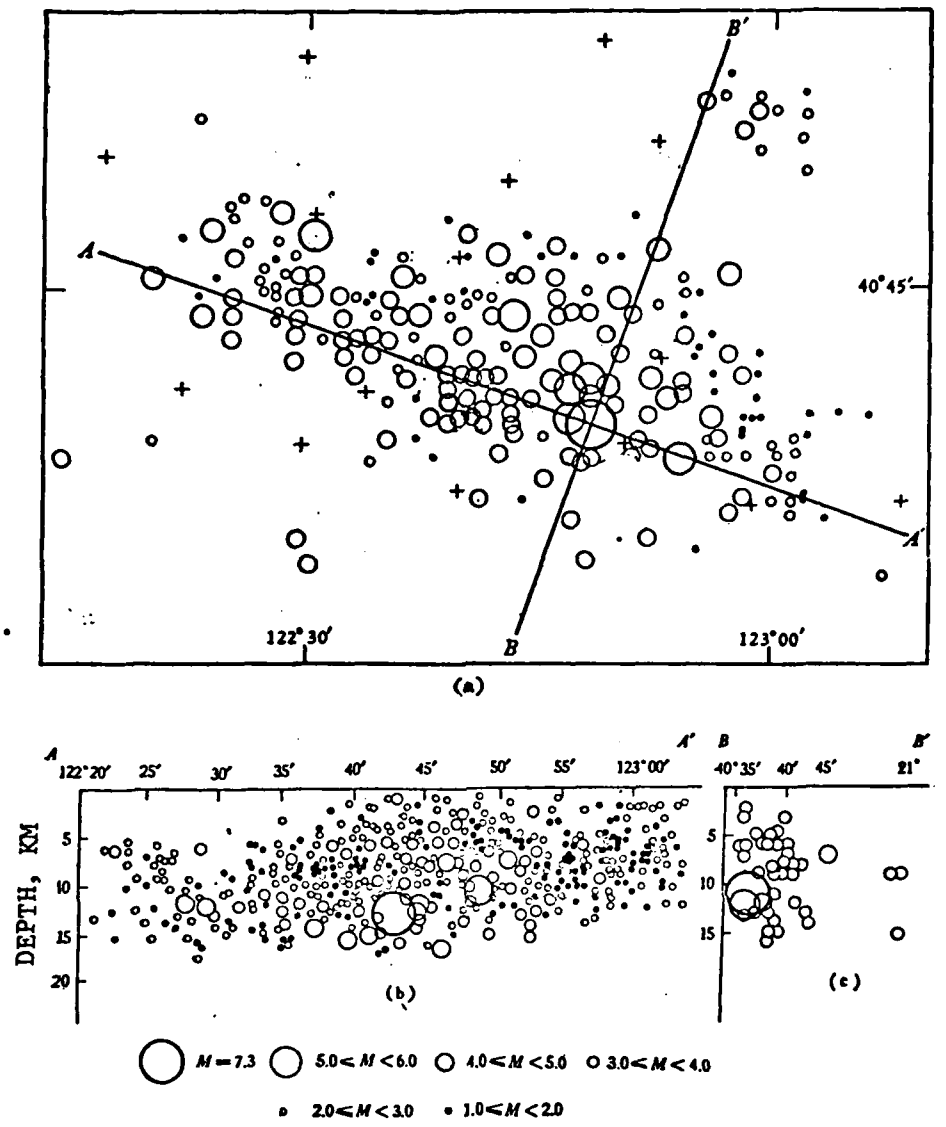

Figure 4. Map shows the distribution of earthquakes of magnitude 2 and greater between February 1 and May 31, 1975 from Gu and others, 1976.

APPENDIX 1

LATE CENOZOIC TECTONICS OF THE TIBETAN PLATEAU

James Ni and James E. York[1]

Department of Geological Sciences, Cornell University
Ithaca, New York 14853

Abstract. Normal faulting interpreted from LANDSAT imagery and fault plane solutions of earthquakes suggest late Cenozoic east-west extension in the Tibetan Plateau. Volcanism and earthquake swarms could be additional evidence for extension, although they are not unique to extensional environments. Normal faulting contrasts with major thrusting along the southern boundary and major strike-slip faulting near the other boundaries of Tibet. The extension may be related to western Tibet being compressed between thrusting on the south and strike-slip faulting on the northwest and consequently spreading along an east-west trend.

Introduction

The Tibetan Plateau (Figure 1) is bounded on the north, south, and west by the Kunlun, the Himalayan, and the Karakorum mountains, respectively. Between 93°E-100°E, ranges trending northwesterly and northerly separate Tibet from southeastern China. The average elevation in the Tibetan Plateau is about 5 km. Although very little published geological and geophysical data on the Tibetan Plateau are available, the Tibetan Plateau is presumably a product of collision of the Indian and Eurasian plates [Gansser, 1964; Dewey and Burke, 1973; Burke et al., 1974; Molnar and Tapponier, 1975]. Stepped river terraces and abnormally large alluvial fans in the mouths of tributaries of the Tsangpo and Sutlej rivers [Li, 1963] suggest that uplift may be still continuing, at least along the southern boundary.

---

[1]Now at Los Alamos Laboratory, Group G-20 MS 676, P. O. Box 1663, Los Alamos, New Mexico 87545.

The geology of Tibet has been summarized by Henning [1916], Norin [1946], Chang [1963], and Burke et al. [1974]. Volcanics of late Cenozoic age, mostly of calc-alkaline type, are widely distributed over Tibet, especially in southern Tibet [Bonvalot, 1892; Henning, 1961; Burke et al., 1974; Kidd, 1975]. This and the presence of fumorolic fields in the Nyenchen Thanghla Mountains imply that the crust of Tibet is hotter than the crust in a stable region.

Available data indicate that late Cenozoic deformation includes strike-slip faulting [Molnar and Tapponier, 1975; Tapponier and Molnar, 1976; York et al., 1976], thrusting and folding in the upper crust and perhaps ductile creep at a deeper level [Dewey and Burke, 1973; Burke et al., 1974], and normal faulting in the Tibetan Himalayas [Gansser, 1964; Bordet et al., 1968]. This paper is primarily concerned with understanding the contemporaneous tectonics through the use of data on seismicity, fault plane solutions, and geological features interpreted from LANDSAT imagery.

Reliable geophysical data for the Tibetan Plateau are scarce. Negative Bouguer gravity and near-zero free air gravity anomalies are reported by Chang and Zeng [1974], which suggest thicker than normal crust and isostatic equilibrium of the Tibetan Plateau. No refraction studies are published to our knowledge. Studies of surface-wave dispersion data show a possible 65- to 70-km thickness of crust under the Tibetan Plateau [Gupta and Narain, 1967; Tung, 1975; Bird and Toksöz, 1977; Chun and Yoshii, 1977]. Studies of Sn and Lg show inefficient propagation along paths that cross Tibet [Molnar and Oliver, 1969; Ruzaikin et al., 1977].

Data

Seismicity

Seismicity in the Tibetan Plateau is high for an intraplate area. Often the seismicity is characterized by swarms of earthquakes with maximum magnitudes

of approximately 6.5. Two large earthquakes ($M \geq 7.8$) have occurred, in 1950 and in 1951. In addition, since 1900 fifteen earthquakes with magnitudes from 7.0 to 7.8 occurred in this region [Shih et al., 1973; York et al., 1976]. Earlier earthquake records in Tibet are rare, mainly because of its low population.

For comparison of the faults interpreted from LANDSAT imagery with earthquakes, epicenters were selected on the basis of a good azimuthal distribution of teleseismic stations. These epicenters were located by the International Seismological Summary (ISS) from 1960 to 1963 and by the International Seismological Centre (ISC) from 1964 to 1975 (Figure 2). Events south of the main central thrust and east of 97°E are not included. The selected epicenters, about 45% of all located earthquakes, represent the most accurately located epicenters.

Fault Plane Solutions

New fault plane solutions were determined for five earthquakes using the first motion of P waves and some S-wave polarizations recorded on long-period instruments of the World-Wide Network of Standardized Seismographs (WWNSS) between 1967 and 1975 (Figure 3). Some of the fault plane solutions (1 to 3) are poorly constrained because of their small magnitude and the unavailability of seismic data from nearby stations. In Figure 2 fault plane solutions of Ritsema [1961], Fitch [1970], Molnar et al. [1973], Ben-Menahem et al. [1974], and Tapponnier and Molnar [1977] are given in addition to these five solutions.

LANDSAT Imagery

The Tibetan Plateau, because it is largely unmapped geologically, provides a good opportunity for the practical use of LANDSAT imagery for obtaining regional geological and tectonic information. The mosaic constructed by

York et al. [1976] at a scale of 1:1,000,000, composed of black and white, band 7 imagery (near infrared, 0.8 to 1.1 μm wavelength), is used for this study. The information extracted from this mosaic was photographically reduced to a 1:4,000,000 scale, and this version was used as the base map.

In this study lineaments on the imagery are interpreted as late Cenozoic faults primarily based on linearity, sharpness of a scarp, and presence of a topographic, tonal or textural difference across the lineament. Characteristics of different types of faulting can be inferred from their geomorphology. Normal faults are indicated by sharp, broken, and en echelon fault traces with average segment lengths of 10 to 20 km. Major strike-slip faults are characterized by long linear traces and can often be readily identified from LANDSAT imagery. Evidence for recent motions along such faults is provided by sharp offsets in the Quaternary alluvium and ponding of streams [York et al., 1976; Tapponnier and Molnar, 1977]. Traces of active thrust faults tend to be very irregular. Recent thrust faults are usually hard to recognize in photo interpretation because low angles of dip create sinuous patterns in map view and many of the patterns are not topographically enhanced by erosional processes.

Volcanics of Neogene to Quaternary age occur extensively in southern and northeastern Tibet [Burke et al., 1974; Kidd, 1975]. Samples gathered in early expeditions, mostly in southern Tibet, are mostly of calc-alkaline type and are of late Cenozoic age [Henning, 1916; Burke et al., 1974; Kidd, 1975]. But these few samples do not imply that all late Cenozoic volcanics throughout Tibet are calc-alkaline. Very large flow sheets resembling plateau basalt can be seen from LANDSAT imagery in northeastern Tibet [Kidd, 1975] (Figure 4), and a few Quaternary basalts are shown on the Geologic Map of China [1976]. The most conspicuous volcanic landforms are shown in Figure 2.

Normal Faulting

The distribution of late Cenozoic normal faults that we mapped from LANDSAT imagery is shown in Figure 2. The widths of larger graben are 10-15 km. Smaller graben are 5-10 km in width and some tens of kilometers long (Figures 5 and 6). Scarps in alluvium, deformed terrace, and dramatic relief leave little doubt that the normal faults are active. The majority of normal faults strike northeast to northwest. Faults tend to be crooked in map plan, sometimes showing a rhomboid or even rectilinear pattern. The graben structures and associated normal faults are more extensively distributed in southern Tibet (Nyenchen Thanghla Mountains and Tibetan Himalayas) than in northern Tibet, and they are not observed south of the high Himalayas, where thrust faults predominate. Although normal faults of the Tibetan Plateau have not been previously mapped based on field work, some resemblance with known normal faults in other continental regions supports our interpretation.

The fault plane solution for the January 19, 1975 earthquake (see also Banghar [1976]) located south of the Karakoram fault indicates a large component of N-S trending normal faulting, although it allows a small component of strike-slip faulting because one of the fault planes is not well constrained. The epicenter lies about 20 km south of and on an extrapolation of a N-S trending normal fault interpreted from LANDSAT imagery (Figure 7). A lake in the graben and a young alluvial fan along the fault trace suggest Quaternary activity on the fault. Aftershocks associated with this earthquake are also located along a N-S trend [Banghar, 1976]. N-S striking normal faults are also known in this region from field study [Hagen, 1969]. A poorly constrained fault plane solution of a March 6, 1966 earthquake [Fitch, 1970] occurred about 200 km southeast of the epicenter of this earthquake (Figure 2) and also shows normal faulting with planes striking north.

The mechanisms of the events of August 16, 1973 and September 8, 1973 (Numbers 3 and 4, respectively, Figure 2) both show some component of normal faulting. The epicenters of these earthquakes are located near normal faults interpreted from LANDSAT imagery (Figure 8) and may be associated with similar structures. A strong component of strike-slip motion is present in these and other fault plane solutions in central and western Tibet. Although the relative amounts of normal and strike-slip motions vary, most solutions are consistent in indicating an approximately horizontal, east-west trending tensional axis.

The epicenter of the earthquake of May 3, 1971 occurs near northwest trending normal faults and graben system nearby (Figures 2 and 9), although the mechanism (which is poorly determined) is nearly pure strike-slip. However, the mechanism is still consistent with approximately east-west extension.

Major Strike-Slip Faulting

Large strike-slip faults near the eastern, western, and northern boundaries of the Tibetan Plateau were previously identified and named the Altyn Tagh fault (Figure 4), the Kunlun fault, and the Kang Ting fault, all with left-lateral displacement, and the Karakoram fault with right-lateral displacement [Molnar and Tapponneir, 1975; York et al., 1976; Tapponnier and Molnar, 1977] (Figure 2). The right-lateral Po Chu fault is newly identified and named in this paper (Figures 2 and 10).

Support for right-lateral motion on the Po Chu fault comes from two fault plane solutions. The earthquake of August 15, 1967 (number 1, Figure 2) occurred near the northwest trending lineaments that parallel the Po Chu fault. The rather poorly constrained fault plane solution shows right-lateral motion on the northwest trending plane. The second fault plane solution is that of the great Assam earthquake of August 15, 1950, which was located about 7 km from

from the Po Chu fault. The large size of the earthquake and the clear trace of the fault on the imagery suggest that the earthquake may have occurred on the fault. Unfortunately, this fault plane solution has been the subject of controversy, mainly because first-motion studies before the deployment of standardized long-period seismographs were sometimes unreliable. Tandon [1955] reported a normal fault plane solution based on the first-motion data reported in the ISS. Chen and Molnar [1977] found that the same ISS data and aftershock locations are consistent with an underthrust dipping gently to the north. However, Ben-Menahem et al. [1974] reviewed all of the available original data regarding the first P motion and aftershock locations and have added surface-wave amplitude studies. They concluded that the fault plane solution showed a strong strike-slip component. Their solution is consistent with right-lateral motion on the Po Chu fault.

Conclusions

Normal faulting interpreted from LANDSAT imagery and fault plane solutions support the hypothesis that there has been east-west extension on the Tibetan Plateau during late Cenozoic. Volcanism and earthquake swarms also occur in Tibet and can be characteristic of extensional environments, although they also can occur in island arcs. In relation to the tectonic activity around the boundaries of Tibet as indicated by geological and geophysical investigations and studies of seismicity and to the uplift of Tibet, the extensional tectonics within Tibet appear minor. Hence we present a model in which the extensional features are a consequence of the major faulting along the boundaries and the uplift.

The extensional tectonics can be explained as resulting from relative eastward motion of the Tibetan Plateau as it is wedged from between the Indian

plate and the stable Tarim Basin (Figure 1). The wedging results primarily because the Altyn Tagh and Karakoram faults converge towards each other in western Tibet. The relative motions on these large faults tend to push the Tibetan Plateau to the east. Fault plane solutions [Yeh et al., 1975] indicate that convergence occurs in the Karakoram mountains. Thus, apparently both convergence there and east-west extension in Tibet occur.

Acknowledgments. We thank W.S.F. Kidd, J. Oliver, B. Isacks, D. Forsyth, and A. Bloom for critically reviewing the paper. We also thank P. Molnar for providing us with all preprints of his work on China, and D. Karig, R. Kay, and D. Turcotte for suggestions and help during the work. This research was supported by the Advanced Research Projects Agency of the Department of Defense and was monitored by the Air Force Office of Scientific Research under Grant No. AFOSR-77-3170. Department of Geological Sciences of Cornell University contribution number 605.

References

Banghar, A. R., Mechanism solution of Kinnau (Himachel Pradesh, India) earthquake of January 19, 1975, Tectonophysics, 31, T5-T11, 1976.

Bem-Menahem, A., E. Aboudi, and R. Schild, The source of the great Assam earthquake--an intraplate wedge motion, Phys. Earth Planet. Interiors, 9, 265-298, 1974.

Bird, P., and M. N. Toksöz, Strong attenuation of Rayleigh waves in Tibet, Nature, 266, 161-162, 1977.

Bonvalot, G., De Paris au Tonkin à traverse le Thibet inconnu, 511 pp., 108 ill., Hatchette, Paris, 1892.

Bordet, P., M. Colchen, D. Krummenacher, P. LeFort, R. Mouterde, and J. M. Rémy, Esquisse géologiques de la Thakkola (Népal Central), C.N.R.S. Paris, 1/75,000, 1968.

Burke, K. C., J. F. Dewey, and W.S.F. Kidd, The Tibetan Plateau, Its significance for tectonics and petrology (abstract), Geol. Soc. Amer. Abstr. Program, 6, 1027-1028, 1974.

Chang, C. F., and S. L. Zeng, Tectonic features of the Mt. Jolmo Lungma region and discussion on the evolution of the Himalayas and the east-west trending mountain ranges in the Tibetan Plateau (in Chinese), 273-299, Geology Volume of Report on the Scientific Expedition to the Mt. Jolmo Lungma Region, Tibet Scientific Brigade of the Chinese Academy of Science, Science Publisher, Peking, 299 p., 1974.

Chang, T., The Geology of China (English transl.), U.S. Dept. Commerce Tech. Services, Jt. Publ., Res. Service, 623 p.(original published 1959), 1963.

Chen, W. P., and P. Molnar, Seismic moments of major earthquakes and the average rate of slip in central Asia, J. Geophys. Res., 82, 2945-2969, 1977.

Chun, K. Y., and T. Yoshii, Crustal structure of the Tibetan Plateau, A surface wave study by a moving window analysis, Bull. Seismol. Soc. Amer., 67, 735-750, 1977.

Dewey, J. F., and K. C.A. Burke, Tibetan, Variscan and Precambrian basement reactivation, Product of continental collisional orogeny, J. Geology, 81, 683-692, 1973.

Fitch, T. J., Earthquake mechanisms in the Himalayan, Burmese, and Andaman regions and continental tectonics in central Asia, J. Geophys. Res., 75, 2699-2709, 1970.

Gansser, A., The Geology of the Himalayas, Wiley Interscience, New York, 289 p., 1964.

Geologic Map of China, Chinese Academy of Geological Sciences (1:4,000,000), Peking, China, 1976.

Gupta, H. K., and H. Narain, Crustal structure in the Himalayan and Tibet Plateau region from surface wave dispersion, Bull. Seismol. Soc. Amer., 57, 235-248, 1967.

Hagen, T., Report on the geological survey of Nepal. Volume 1 -- Preliminary reconnaissance, Soc. Helv. Sci. Nat. Mem., 86, No. 1, 185 p., Zurich, 1969.

Henning, A., Zur petrographie und geologie von Sudwesttibet, in Southern Tibet, Vol. V, Kung. Boktryekeriet, P. A. Norstedt and Sonar, Stockholm, 1916.

Kidd, W.S.F., Widespread late Neogene and Quaternary alkaline volcanism on the Tibetan Plateau (abstract), EOS Trans. AGU, 56, 453, 1975.

Li, P., Certain data on neotectonic movement in Tibet, in Works of the First Conference on Neotectonics in China, ed. V. N. Paulinov, pp. 209-215, 1963.

Molnar, P., T. J. Fitch, and F. T. Wu, Fault plane solutions of shallow earthquakes and contemporary tectonics in Asia, Earth Planet. Sci. Lett., 19, 101-112, 1973.

Molnar, P., and J. Oliver, Lateral variations of attenuation in the mantle and discontinuities in the lithosphere, J. Geophys. Res., 74, 2648-2682, 1969.

Molnar, P., and P. Tapponier, Cenozoic tectonics of Asia: Effects of a continental collision, Science, 189, 419-426, 1975.

Norin, E., Geological Explorations in Western Tibet, Reports from the Scientific Expedition to the Northwestern Provinces of China under the Leadership of Dr. Sven Hedin, 29, III Geology 7, Tryckeri Aktiebolaget Thule, Stockhold, 1946,

Ritsema, A. R., Some 1951 earthquake mechanisms based on P and PKP data, Geophys. J. R. Astron. Soc., 5, 254-258, 1961.

Ruzaikin, A. I., I. L. Nersesov, V. Z. Khalturin, and P. Molnar, Propagation of Lg and lateral variations in crustal structure in Asia, J. Geophys. Res., 82, 307-316, 1977.

Shih, C. L., W. L. Huan, H. R. Wu, and X. L. Cao, On the intensive seismic activity in China and its relation to plate tectonics (in Chinese) Scientia Geol. Sinica, 4, 281-293, 1973.

Tandon, A. N., Direction of faulting in the great Assam earthquake of August 15, 1950, Ind. J. Meteor. Geophys., 6, 61-64, 1955.

Tapponnier, P., and P. Molnar, Slip line field theory and large-scale continental tectonics, Nature, 264, 319-324, 1976.

Tapponnier, P., and P. Molnar, Active faulting and Cenozoic tectonics in China, J. Geophys. Res., 82, 2905-2930, 1977.

Tung, J.P.Y., The surface wave study of crustal and upper mantle structures of mainland China, Ph.D. Thesis, University of Southern California, 331 p., 1975.

Yeh, H., Y. S. Liang, L. Q. Shen, and H. F. Xiang, The analysis of the recent tectonic stress of the Himalaya Mountains arc and its vicinities, Scientia Geol. Sinica, No. 1, 32-48, 1975.

York, J. E., R. Cardwell, and J. Ni, Seismicity and Quaternary faulting in China, Bull. Seismol. Soc. Amer., 66, 1983-2001, 1976.

FIGURE CAPTIONS

Fig. 1. Simplified map of geography and tectonics in the Tibetan Plateau. Heavy lines represent major active faults. Heavy dashed line represents Indus suture. From north to south large open arrows show relative motion between the Tarim Basin, the Tibetan Plateau, and the Indian plate. Location and form of graben are approximate.

Fig. 2. Seismo-tectonic map of the Tibetan Plateau, with faults and type of faulting interpreted from LANDSAT imagery. Thrusts with solid barbs are from Tapponnier and Molnar [1977]. Thrust with open barbs are inferred from analysis of imagery. Solid lines represent active faults; dashed lines represent most conspicuous lineaments. Line with hachures on one side are normal faults. Arrows with solid heads indicate direction of motion supported by fault plane solutions or surface faulting of earthquakes from Molnar and Tapponnier [1975] and York et al. [1976]. Arrows with open heads indicate direction inferred from photo interpretation. Large open circles represent all selected earthquakes (see text) with $5 \leq m_b \leq 6\text{-}1/4$; small open circles, $4 \leq m_b \leq 5$. The fault plane solutions numbered 1 through 5 correspond to events reported in Figure 3. Previously reported solutions are indicated by letters next to the solutions. R is from Ritsema [1961], F from Fitch [1970], M from Molnar et al. [1973], B from Ben-Menahem et al. [1974], and T from Tapponnier and Molnar [1977]. Solid areas are most conspicuous volcanic land forms of Neogene to Quaternary age observed on LANDSAT imagery.

Fig. 3. New focal mechanism solutions for crustal earthquakes in Tibet, using lower hemisphere projections. Polarities of P-waves first motions are given by large and small solid circles for clear and weak compression, respectively; large and small open circles for clear and weak dilatation, respectively; and crosses for uncertain polarization. S-wave polarization is indicated by arrows.

Tick marks on nodal planes give the locations of poles to one of the nodal planes. P and T are the location of maximum and minimum compression, respectively.

Fig. 4. Large dissected volcanic flows at A and B. Drainage has developed atop both mesas indicating that parts may be older than Quaternary. Volcanic cone at D. Snow and ice-covered anomalously high topographic features around G and H may be Quaternary volcanoes (W.S.F. Kidd, personal communication, 1977). Center of image is approximately at 35.6°N, 89.4°E (LANDSAT image No. 1215-04094).

Fig. 5. Arrows indicate normal faults in the left portion of the photo. Notice the horst and graben feature and sharp tonal and textural contrast across the fault. Center of image is approximately 31.4°N, 82.5°E (LANDSAT image No. 1507-04304).

Fig. 6. North-south striking normal faults indicated by arrows on eastern flank of the graben at the center of the photo. Its broken but short, linear trace is clearly seen here. At A an intrusion of granite (Tertiary age according to Geologic Map of China [1976] is cut by the fault. Center of image is approximately 29.0°N, 86.4°E (LANDSAT image No. 1198-04172).

Fig. 7. Earthquake of January 19, 1975 and its fault plane solution. Young alluvial fan has formed along fault scarp at F. Arrow points to the north-south trending normal fault. Karakoran fault lies between arrows. Center of image is approximately at 32.9°N, 78.8°E (LANDSAT image No. 1096-04501).

Fig. 8. Earthquakes of August 16, 1973, and September 8, 1973, and their fault plane solutions. Open circles are locations of earthquake epicenters. Arrows indicate normal faults in nearby areas. A domal feature located at D and a circular lake at C are perhaps suggestive of volcanic origins. Center of image is approximately 33.0°N, 87.1°E (LANDSAT image No. 1144-04160).

Fig. 9. Earthquake of May 3, 1971, and its fault plane solution. Arrows indicate normal faults. Center of image is approximately at 30.5°N, 84.3°E (LANDSAT image No. 1056-04273).

Fig. 10. LANDSAT mosaic of Po Chu fault (named after Po Chu River). The name of this fault is not official. The Po Chu River follows the fault along short straight segments. Fault scarps at S and L. Center of image is approximately at 28.8°N, 96.6°E (LANDSAT image No. 1461-03343).

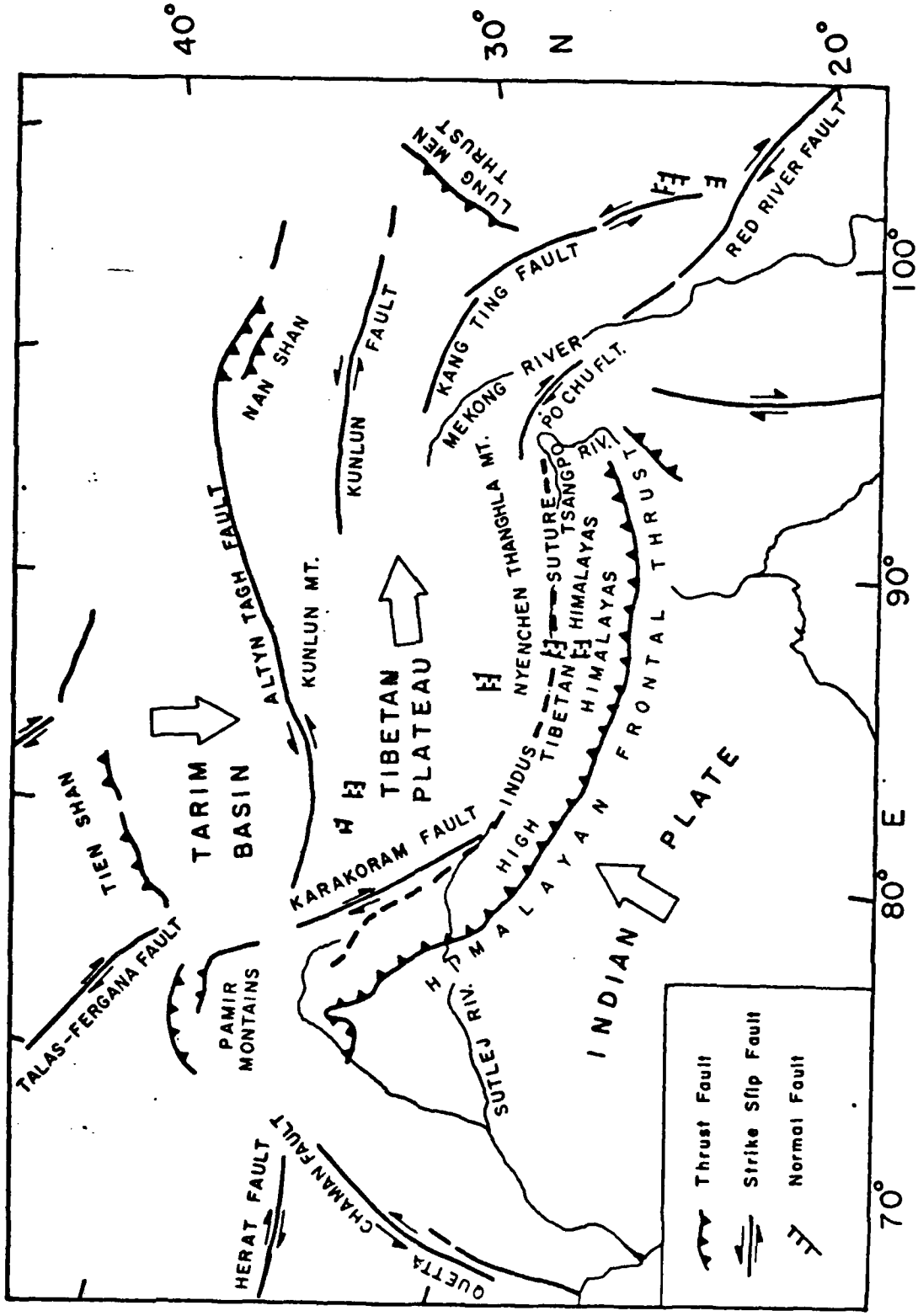
40°
30°
N
20°
100°
90°
80° E
70°
LUNG MEN THRUST
RED RIVER FAULT
KANG TING FAULT
MEKONG RIVER
PO CHU FLT.
NAN SHAN
KUNLUN FAULT
ALTYN TAGH FAULT
KUNLUN MT.
NYENCHEN THANGHLA MT.
SUTURE
TSANGPO RIV.
HIMALAYAS
TIBETAN HIMALAYAS
TIBETAN PLATEAU
TARIM BASIN
TIEN SHAN
KARAKORAM FAULT
INDUS
HIGH
HIMALAYAN FRONTAL THRUST
INDIAN PLATE
TALAS-FERGANA FAULT
PAMIR MONTAINS
SUTLEJ RIV.
HERAT FAULT
CHAMAN FAULT
QUETTA
Thrust Fault
Strike Slip Fault
Normal Fault

Figure 1

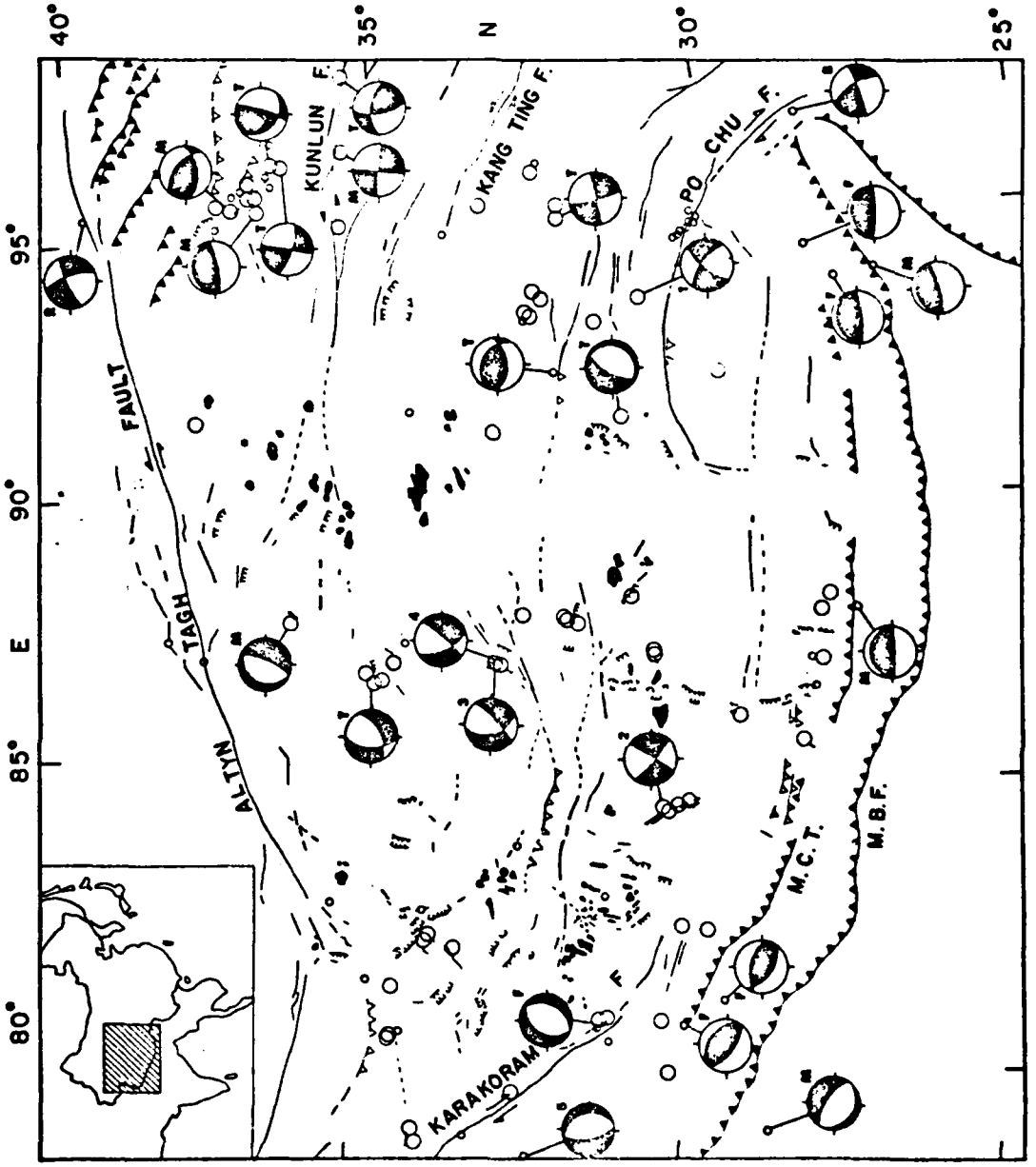
40°
35°
N
30°
25°
95°
90°
E
85°
80°
KUNLUN F.
KANG TING F.
PO CHU F.
FAULT
TAGH
ALTYN
M.C.T.
M.B.F.
KARAKORAM

Figure 2

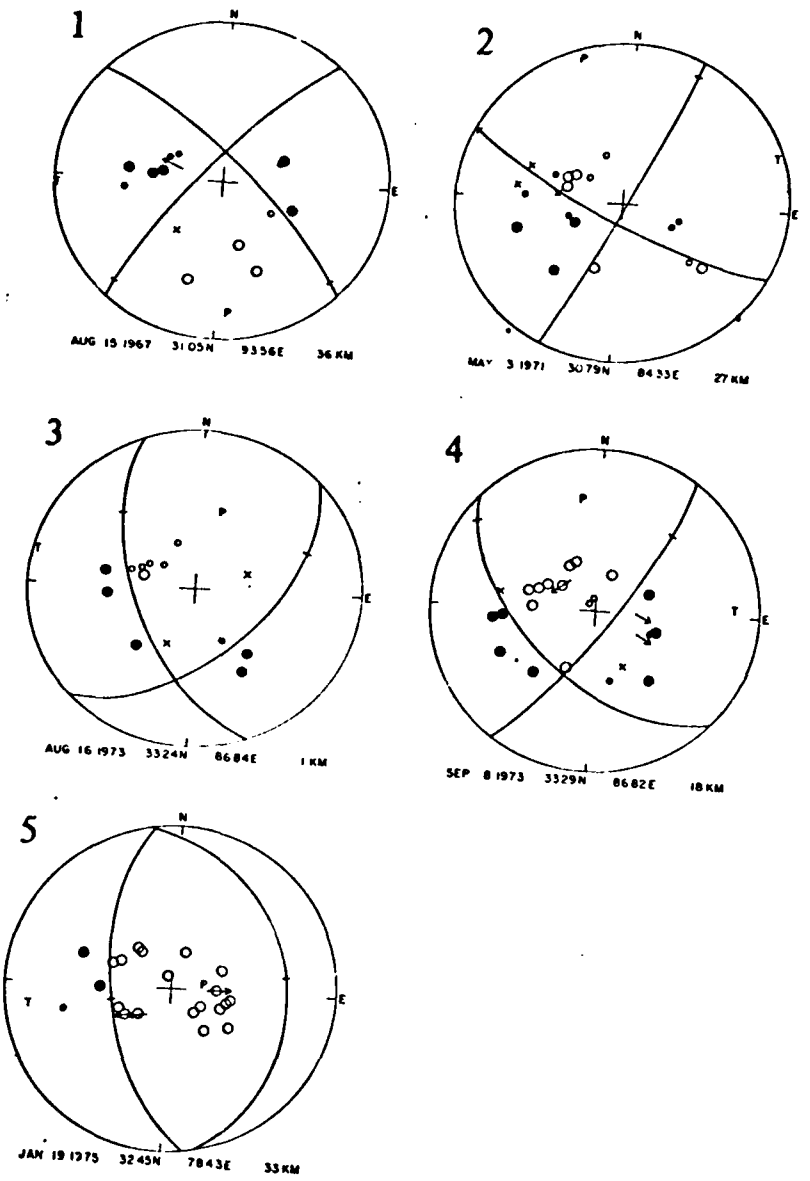
1
N
E
P
AUG 15 1967 31.05N 93.56E 36 KM
2
N
P
T
E
MAY 3 1971 30.79N 84.33E 27 KM
3
N
P
T
E
AUG 16 1973 33.24N 86.84E 1 KM
4
N
P
T
E
SEP 8 1973 33.29N 86.82E 18 KM
5
N
T
P
E
JAN 19 1975 32.45N 78.43E 33 KM

Figure 3

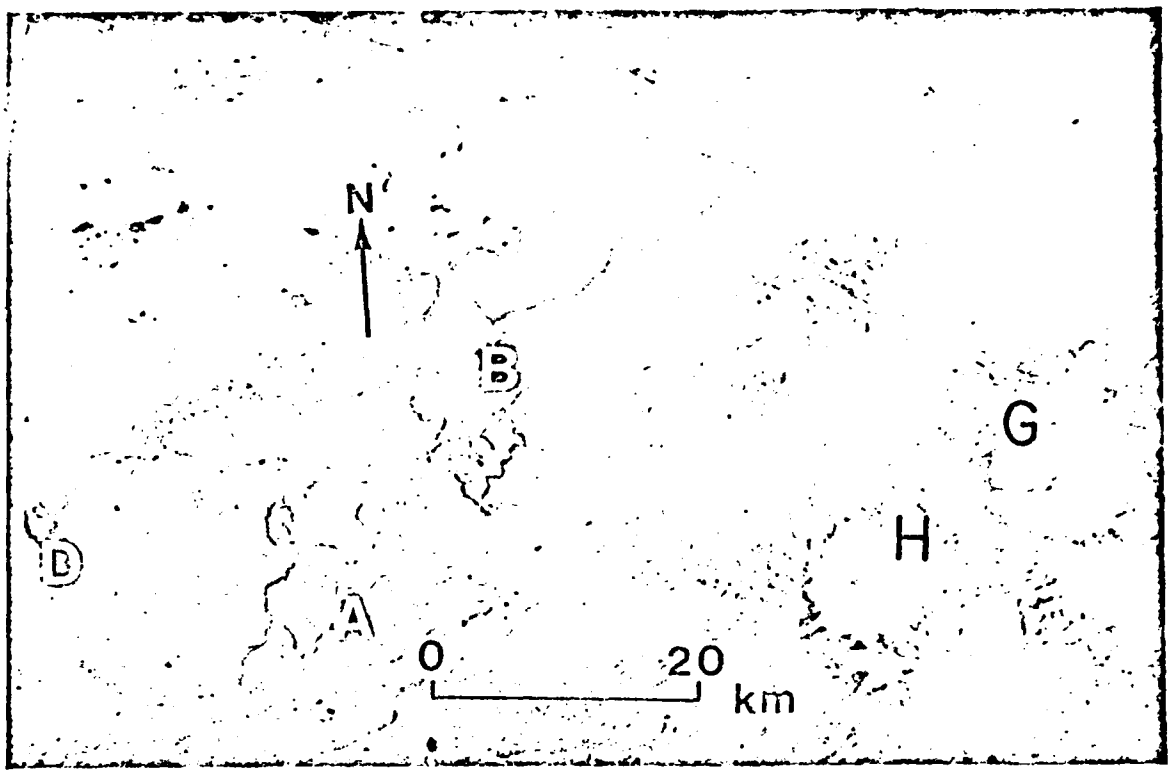

Figure 4

Figure 5

Figure 6

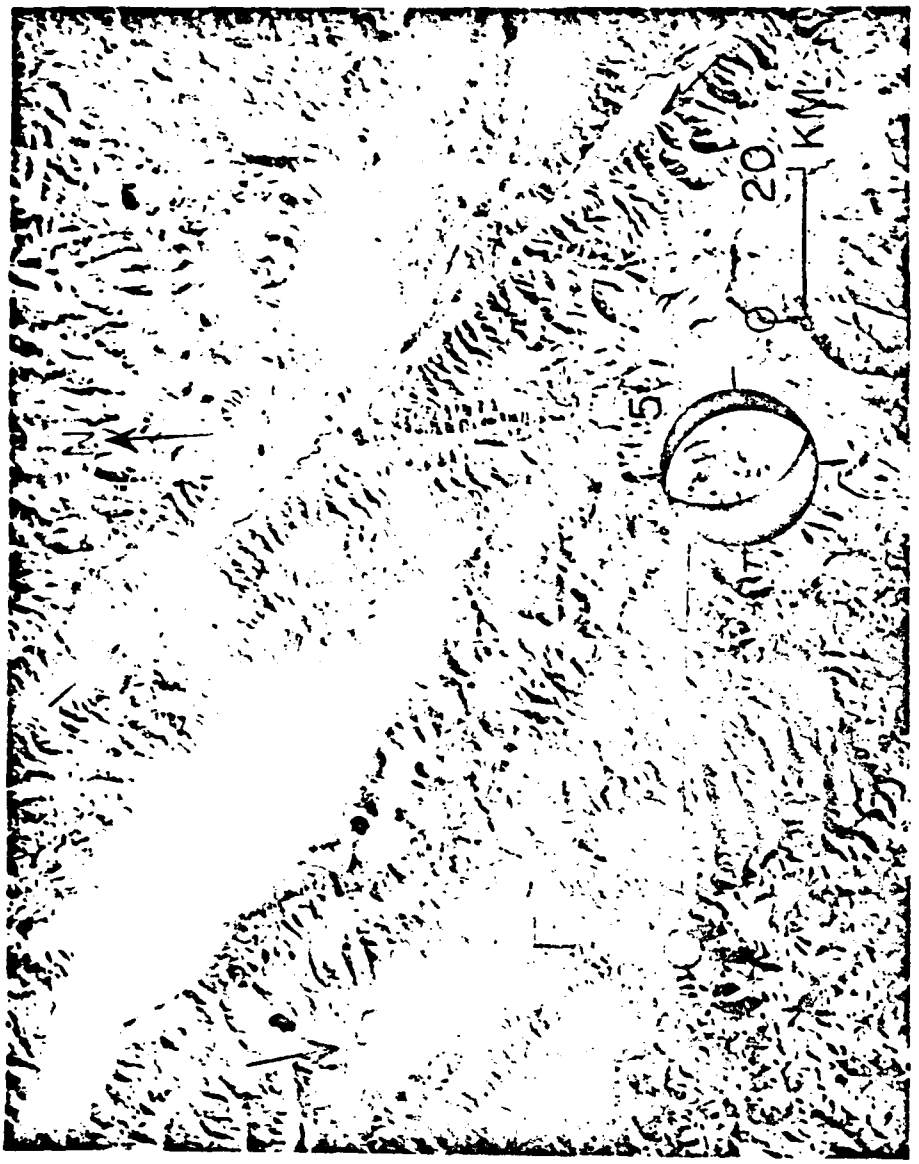

Figure 7

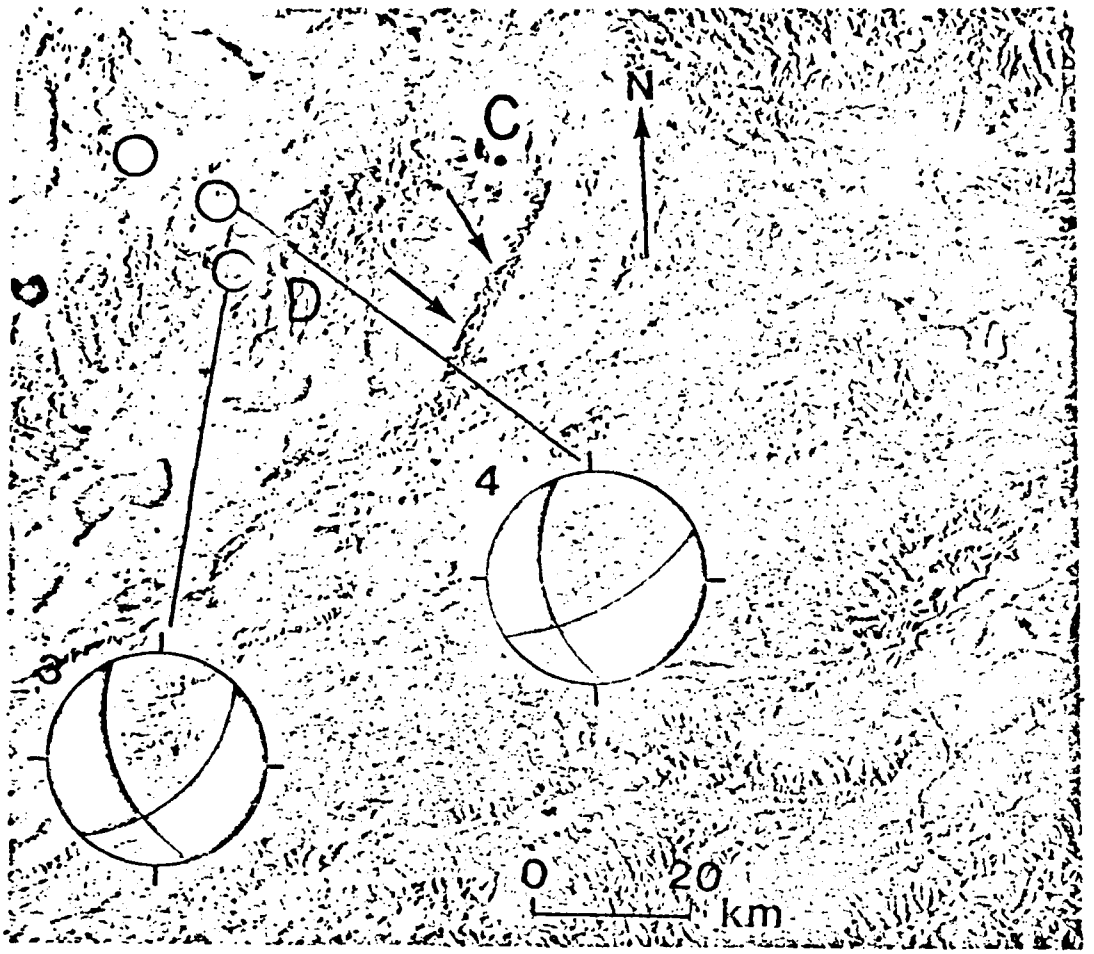

Figure 8

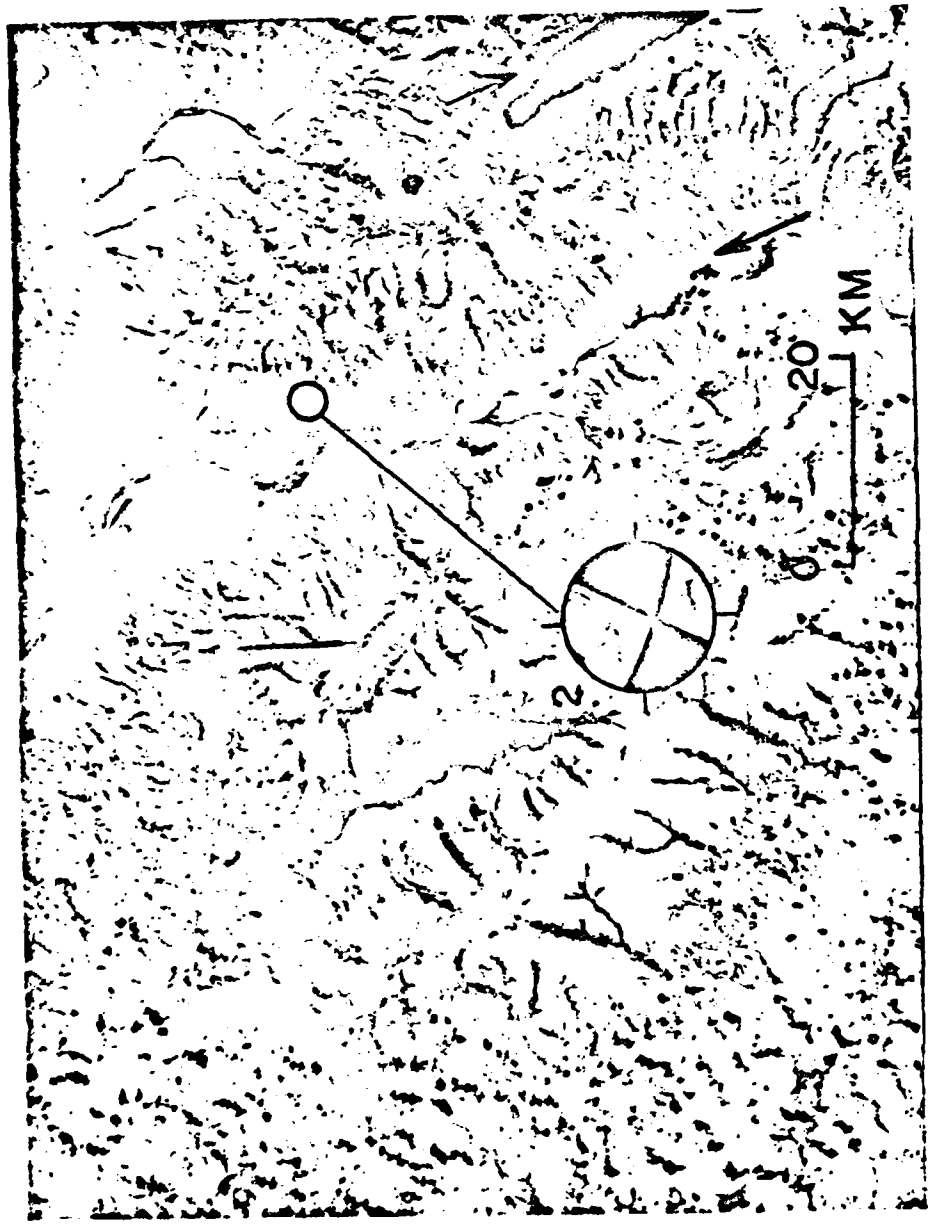

Figure 9

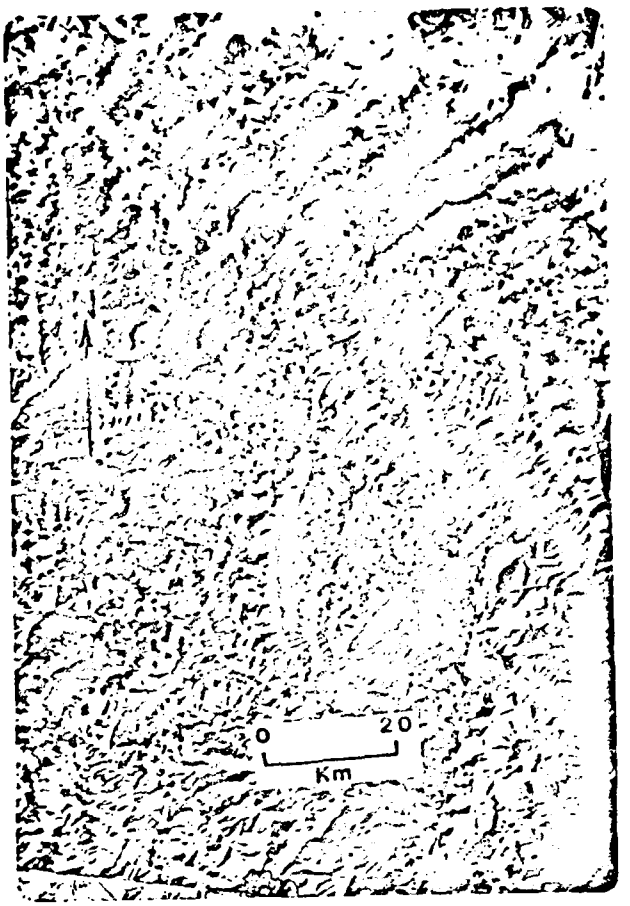

Figure 10

APPENDIX 2

CONTEMPORARY TECTONICS IN THE TIEN SHAN REGION

James Ni
Department of Geological Sciences
Cornell University
Ithaca, New York 14853

ABSTRACT

Fault plane solutions of recent earthquakes, along with published fault plane solutions, geologic data from field reports, and faults interpreted from LANDSAT imagery indicate major thrust faulting in the Tien Shan region. For most of the fault plane solutions compressive stress axes are nearly horizontal and trending approximately N-S, perpendicular to the trend of the Tien Shan fold belts. Contemporary tectonics of the Tien Shan region can be interpreted as resulting from convergence of the Indian and Eurasian plates.

INTRODUCTION

The Tien Shan mountains rise abruptly above the northern border of the Tarim basin and extend westward into the Turanian lowland. They are offset in the middle by the Talaso-Fergana right-lateral strike-slip fault (Fig. 1). The Tien Shan mountains consist of parallel, approximately east-west trending, horst blocks which are often separated by wide latitudinal valleys [1]. The structure of the major portion of Tien Shan was formed during the Hercynian Orogeny [2]. The present high elevation of the Tien Shan mountains is a result of very recent tectonism [1,3,4]. Although the neotectonic structure in this region appears to have been inherited from late Paleozoic structures [5], few examples of large ancient faults which evolved in the Paleozoic are still active [5]. Hence some of the recent faults in Tien Shan region may be independent of older structures.

Previous tectonic and seismic studies show positive correlations between epicenters of strong earthquakes and major structures in the southern Tien Shan region [5,6,7, 8,9,10]. Fault plane solutions indicate an approximately horizontal north-south orientation of the P axes [4,11,12].

In this discussion, recent seismicity and LANDSAT imagery in the Tien Shan region are used to provide information on the relationship between neotectonics and earthquake occurrence.

DATA

Seismicity

Seismicity in the Tien Shan region is very high and is characterized by numerous great earthquakes [7,10]. In order to facilitate comparison of neotectonic structures with earthquakes, epicenters located by the International Seismological Summary (ISS) from 1960 to 1963 and by the International Seismological Center (ISC) from 1964 to 1976 are plotted on Figure 2.

Fault Plane Solutions

New fault plane solutions were determined for twelve earthquakes using the first motion of P waves and some S wave polarizations recorded on long-period instruments of the World-Wide Network of Standardized Seismographs (WWNSS) between 1971 and 1974 (Fig. 3) (Table 1). In Figure 1 these solutions as well as those of Molnar et al., Moskvina and Soboleva [4,9] are given.

Discussion

As shown in Figure 2, the majority of crustal earthquakes occur in the southern part of the Tien Shan Mountains, extending approximately in a latitudinal direction and located southeast of the Issyk-Kul Lake. About 60% of all located crustal events occur along the southern Tien Shan seismic zone. Numerous historical, catastrophic earthquakes have occurred here [7]. The most active section of the southern Tien Shan seismic zone coincides well with the Pamir Foredeep

which is characterized by intensely folded and faulted Cenozoic sediments [3]. High angle reverse faults, strike-slip faults and normal dip-slip faults are known in this region [13,14].

During the months of August and September, 1974, a major earthquake swarm occurred in southwestern Tien Shan near the China-USSR border. This swarm is of main shock-aftershock sequence type. The main shock occurred at 01 hours, August 11, 1974 with M = 6.2 (Mb). Fault plane solutions for the main shock and two aftershocks (20 hrs and August 27, 1974) (Fig. 3) show large components of strike-slip faulting with some thrusting. Although high angle faults striking northeast and intensely folded beds are clearly seen on the LANDSAT imagery (Fig. 4), it is difficult to distinguish between the fault and the auxilliary plane because of the lack of field data in the epicentral region following the occurrence of these swarms. However, the aftershocks associated with main events are located on a narrow strip approximately 40 km in length and 15 km wide (Fig. 5). The trend of the aftershock zone is nearly NW-SE. Therefore it is probable that the fault plane strikes approximately 330°. The fault plane solution for the 21 hr, August 11, 1974 earthquake shows a large component of normal faulting (Fig. 3). Although normal faults striking approximately north and northwest are observed nearby (Fig. 4), nevertheless it appears that block faulting at depth may be associated with this earthquake.

Fault plane solutions for the earthquakes of March 23, 1971, January 15, 1971, June 16, 1971, January 15, 1972, April 9, 1972, June 2, 1973, and three previously determined fault plane solutions by Molnar et al [4] show a large component of thrusting. Although the relative amounts of the strike-slip component vary, most solutions show consistent northeast trending fault planes. Northeasterly trending thrust faults are reported by an early field study [1]. A recent geological study indicates that these thrust faults are dipping 30° to 80° northwest, along the foothills of the southern Tien Shan Mountains east of the Talaso-Fergana fault [15]. Northwest trending high angle dip-slip faults are clearly seen on LANDSAT imagery

(Fig. 6). These faults are also known by field geophysical observations [15]. Microearthquake data with good depth control shows that faulting occurs on both northeast and northwest striking faults [15].

Moskvina and Soboleva [9] determined fault planes for ten crustal earthquakes in the extreme southwestern Tien Shan region (approximately 38.5°N, 69°E) (see examples in Fig. 1) and found that thrust faulting was also the common mode of deformation. However, in contrast with the north-south trending P-axes indicated by fault plane solutions in other parts of Tien Shan, here the P-axes are oriented northwest to southeast. These stress orientations are consistent with NE-trending faults and folds which follow the bend of Pamir arching structure.

The great Talaso-Fergana strike-slip fault cuts across the Tien Shan range. It may have a maximum lateral displacement of approximately 250 km since its initiation during late Paleozoic times [14]. The fault plane solution for the May 10, 1971 earthquake is consistent with motion observed along the fault (Fig. 1). The transition of the Talaso-Fergana transcurrent faults into latitudinal overthrust faults has been shown by Wallace [16]. The earthquake of October 26, 1971 was located approximately 15 km west of the Talaso-Fergama fault. Its fault plane solution shows a large thrust component which is consistent with the orientation of the latitudinal thrust faults nearby.

CONCLUSIONS

Seismic data show that the principal earthquakes zones of the Tien Shan region are clearly related to the neotectonic structures. Fault plane solutions of earthquakes, geologic data from field reports, and faults deduced from LANDSAT imagery indicate that the neotectonics of the southern Tien Shan region are dominatd by thrust faulting in response to approximately north-south compression. The southeastern Tien Shan region is characterized by northward thrusting. In contrast, the southwestern Tien Shan region (Pamir Foredeep) is characterized by southward thrusting. Between these two major thrust belts the Talaso-Fergana right lateral strike-slip fault appears to be absorbing the differential horizontal shortening.

ACKNOWLEDGEMENTS

The author wishes to thank Peter Molnar for critically reviewing this paper and Muawia Barazangi and Selena Billington for their helpful suggestions. This research was partially supported by the Advanced Research Project Agency of the Department of Defense and was monitored by the Air Force Office of Scientific Research and Grant No. AFOSR-77-3170.

This is Cornell University Department of Geological Sciences Contribution Number 617.

REFERENCES

1. E. Norin, Geologic reconnaissance in the Chinese Tien-Shan, in reports from the scientific expedition to the northwestern provinces of China under the leadership of Dr. Sven Hedin, publ. 16, IV, Geology 6 (1941), Trycheri Aktiebolaget Thule, Stockholm.
2. V.S. Burtman, Structural geology of Variscan Tien Shan, USSR, Am. Jour. Sci., 275A (1975), 157-186.
3. I.E. Gubin, Lecture notes on basic problems in seismotectnoics, Intern. Inst. Seism. Earthquake Eng., Tokyo, Japan (1967), 195 p.
4. P. Molnar, T.J. Fitch, and F.T. Wu, Fault plane solutions of shallow earthquakes and contemporary tectonics in Asia, Earth Planet. Sic. Lett., 19 (1973) 101-112.
5. V.M. Knauf, Relation between regional seismic zones and premesozoic structures of the Tien Shan, Bull., (Izv.) Earth Physics, no. 7 (1973), 35-45, Acad. Sci. USSR.
6. V.S. Krestnikov, On the connection between the geological and seismic phenomena in the Tyan-Shan, (in Russian), Byull. Soveta po seismologii, no. 3 (1957).
7. N.A., Vvedenskaya,The earthquake of Central Asia, in Earthquakes in the USSR, Aca., Sci., USSR, English translation by U.S. Atomic Energy Comm., (1961), 351-393.
8. Z.L., Shi, W.L. Huan, H.R. Wu, and Y.L. Cao, On the intensive seismic activity in China and its relation to plate tectonics (in Chinese), Scientia Geol., Sinica 4 (1973), 281-293.
9. A.G. Moskvina, and O.V. Soboleva, A theroretical model of a focus and the macro-seismic earthquake field, Bull. (Izv.), Acad. Sci. USSR, Earth Physics, No. 9 (1973), 17-28.
10. J.E. York, R. Cardwell, and J. Ni, Seismicity and Quaternary faulting in China, Bull. Seism. Soc. Am. 66 (1976), 1983-2001.
11. E.I. Shirokova, General features in the orientation of principal stresses in earthquake foci in the Mediterranean-Asian seismic belt, Bull. Acad. Sci. USSR, Earth Physics 1 (1967), 23-36.

12. B.K. Rastogi, Source mechanism studies of earthquakes and contemporary tectonics in Himalaya and nearby regions, Bull. Inter. Inst. Seism. Earthquake Engr., 14 (1976), 99-134.

13. I.E. Gubin, The Garm earthquake of 1941 (in Russian), Publ. Acad. Sci., USSR Stalingrad (1943).

14. V.S. Burtman, On the Talaso-Fergana wrench-fault (in Russian), Akad. Nauk. SSSR Izv., ser. geol., no. 12 (1961), 37-48.

15. Y.M. Liu, H. Yao, and H.N. Chou, Analysis of the characteristics and trends of seismic activities in the Keping rupture zone in Sinkiang, China, Acta Geophys. Sinica 18 (1975), 39-51.

16. R.E. Wallace, The Talaso-Fergana fault, Kirgiz and Kazakh, USSR, Earthquake Information Bull. 8 (1976), 5-13.

17. Chinese Academy of Geological Sciences, Geologic map of Asia (1:5,000,000), Peking, China (1976).

18. P. Tapponnier and P. Molnar, Active faulting and Cenozoic tectonics in China, J. Geophys. Res. 82 (1977), 2905-2930.

FIGURE CAPTIONS

Figure 1: Fault plane solutions and major faults of the Tien Shan region. Equal area lower hemisphere projections of both new and published (m from Molnar et al. [4], s from Moskvina and Soboleva [9]) fault plane solutions. Black quadrants denote compressional first-motion of p-waves. Inward arrows represent horizontal projection of P-axes (maximum compressive stress); outward arrows represent T-axes (minimum compressive stress). Fault and type of faulting are from [10,17,18].

Figure 2: Seismicity of Tien Shan region. Circles represent focal depth of <70 kilometers. Triangles represent focal depth of 70 kilometers but <300 kilometers. Large open circles and triangles represent epicenters with $5 \leq$ Magnitude <6.3. Small open circles and triangles represent epicenters with $4 \leq$ Magnitude <5. See text for data sources. Solid lines represent faults. Legend is the same as for Figure 1.

Figure 3: New focal mechanism solutions for earthquakes in Tien Shan area, using lower hemisphere projections. Polarities of P-wave first motions are given by large and small solid circles for clear and weak compression, respectively; large and small open circles for clear and weak dilatation, respectively; and solid and open squares for compression and dilatation respectively reported by ISC from nearby stations. Cross-marks on nodal planes give the locations of poles to the nodal planes. P and T are the location of maximum and minimum compressive stress axes respectively.

Figure 4: Epicenters of the August 11, 1974 earthquake (solid circle represents main shock) and its aftershocks. Large open circles and small open circles represent $5 \leq$ Magnitude <6.3 and $4 \leq$ Magnitude <5 respectively.

Figure 5: LANDSAT image (no. 2673-04540) showing (1) highly faulted and folded Pamir Foredeep between A and B, and (2) High angle dip-slip faults, indicated by arrows. Notice the sharp tonal, topographic and textural difference across these faults. Circles represent epicenters of earthquakes which are the same as of Figure 4.

Figure 6: LANDSAT image (no. 2167-04534) showing high angle fault between C and D. Legend for circles are same as for Figure 4. Notice the folded beds on the foothills of southern Tien Shan Mountains resulting from northward dipping thrust faults (between arrows).

TABLE 1. FOCAL MECHANISM SOLUTIONS

Day	Mo.	Yr.	Epicenter Lat(N) degrees	Epicenter Long(E) degrees	Depth km	Pole of 1st Nodal Plane Trend	Pole of 1st Nodal Plane Plunge	Pole of 2nd Nodal Plane Trend	Pole of 2nd Nodal Plane Plunge	Axis of Compression (P) Trend	Axis of Compression (P) Plunge	Axis of Tension (T) Trend	Axis of Tension (T) Plunge	Null Axis (B) Trend	Null Axis (B) Plunge
23	Mar	71	41.42	79.20	14	342	46	172	45	347	1	255	84	63	6
10	May	71	42.58	71.29	13	318	41	216	14	3	17	257	50	112	45
15	Jun	71	41.39	79.18	96	317	21	198	52	160	18	277	54	60	32
16	Jun	71	41.49	79.29	14	326	21	224	30	185	6	279	37	85	53
28	Oct	71	41.88	72.35	15	156	52	342	38	160	6	0	83	251	3
15	Jan	72	40.17	78.96	8	345	20	192	68	172	24	330	65	345	20
9	Apr	72	42.09	84.58	21	346	3	166	87	167	42	348	47	77	0
2	Jun	73	44.14	83.60	20	6	6	186	84	6	38	186	52	96	0
11	Aug	74	39.34	73.76	7	324	24	223	24	183	0	273	36	92	53
11	Aug	74	39.44	73.67	41	328	29	219	31	183	1	272	46	92	45
11	Aug	74	39.46	73.62	26	42	22	236	68	34	66	227	22	135	5
27	Aug	74	39.52	73.82	14	21	5	290	10	355	10	245	4	147	78

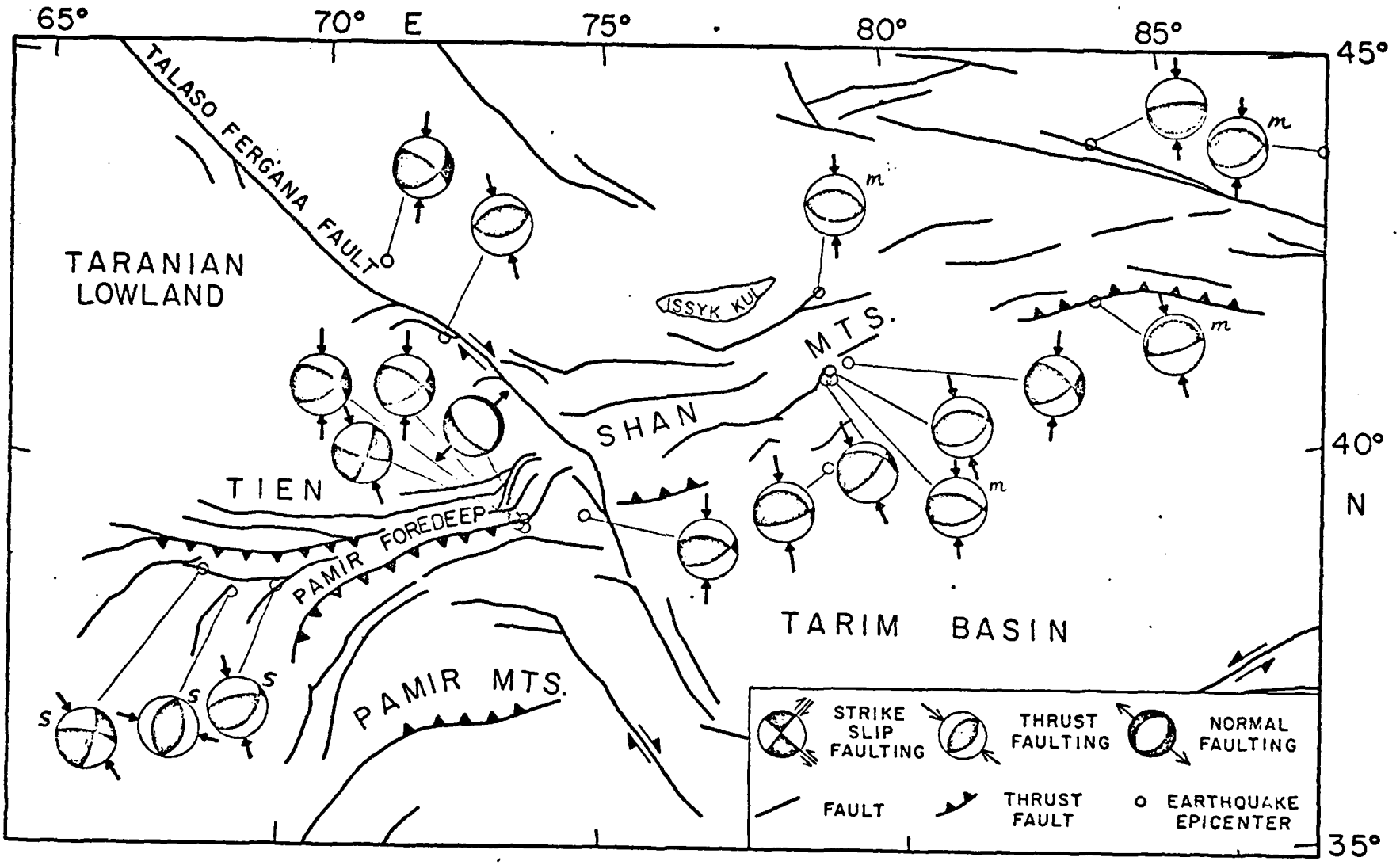
65°
70° E
75°
80°
85°
45°
40°
N
35°
TALASO FERGANA FAULT
TARANIAN LOWLAND
ISSYK KUL
TIEN SHAN MTS.
TIEN
PAMIR FOREDEEP
PAMIR MTS.
TARIM BASIN
m
s
STRIKE SLIP FAULTING
THRUST FAULTING
NORMAL FAULTING
FAULT
THRUST FAULT
EARTHQUAKE EPICENTER

Fig. 1

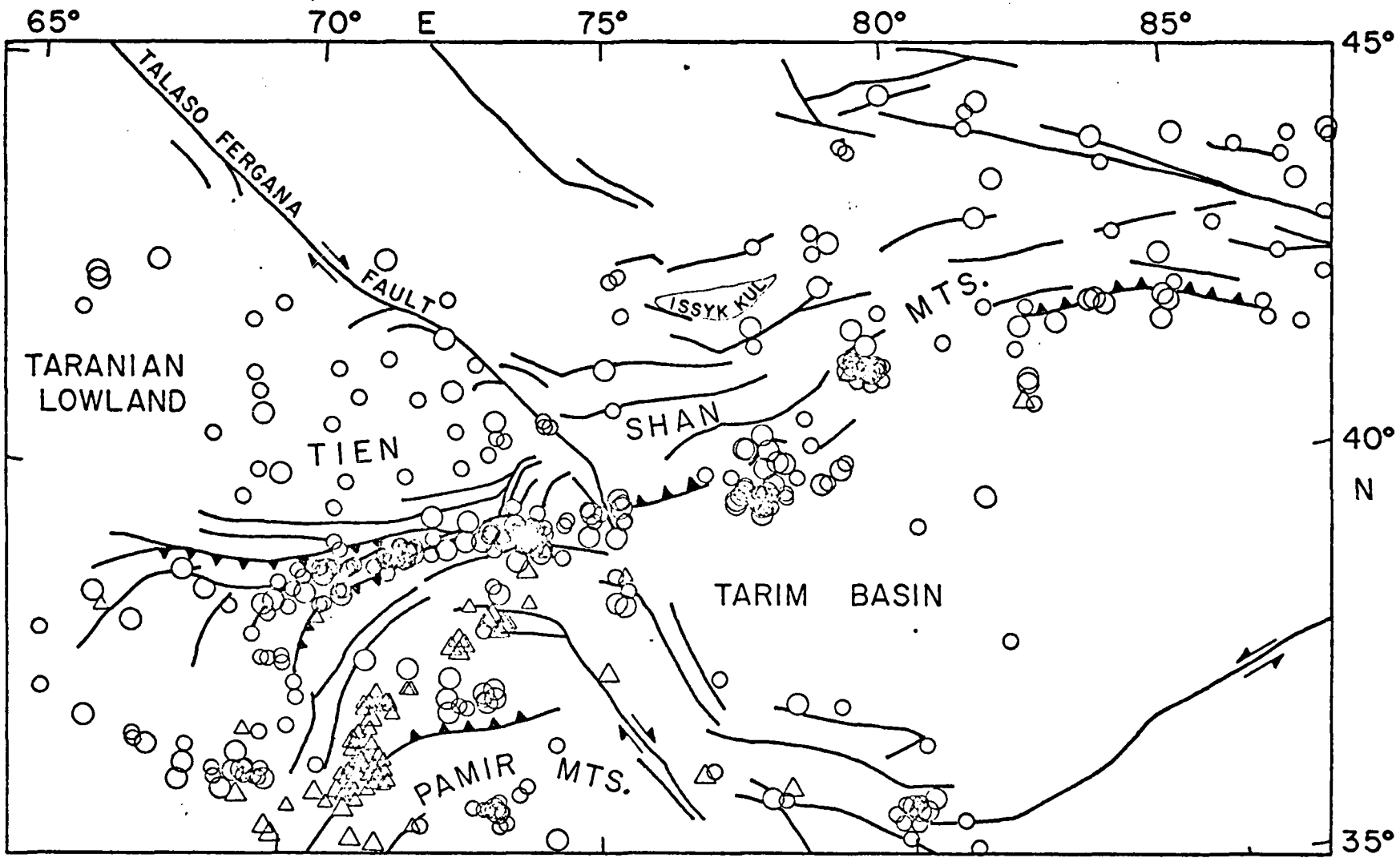
65°
70°
E
75°
80°
85°
45°
40°
N
35°
TALASO FERGANA
FAULT
ISSYK KUL
MTS.
TARANIAN
LOWLAND
TIEN
SHAN
TARIM BASIN
PAMIR MTS.

Fig 2

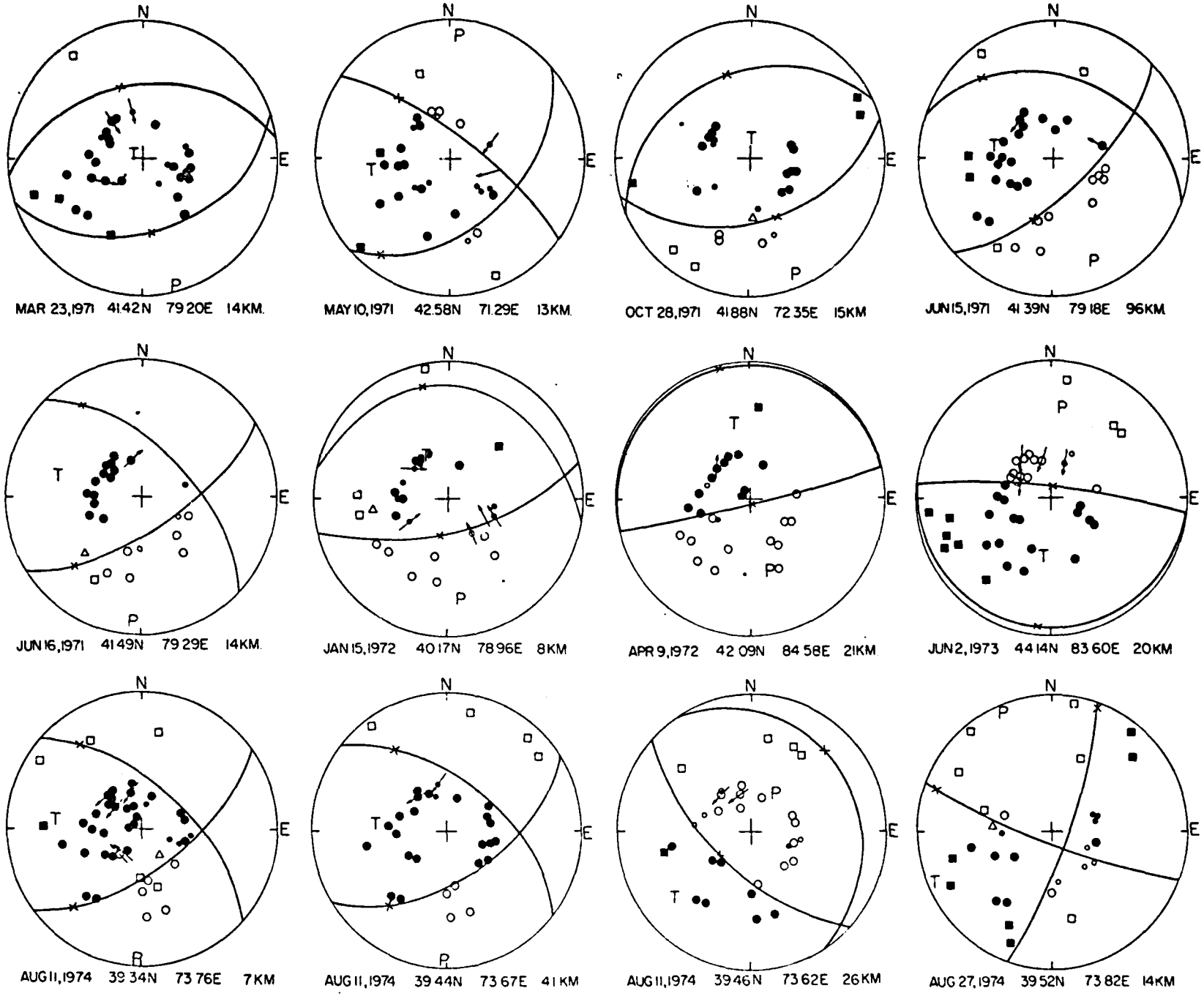
N
E
P
T
MAR 23,1971 41.42N 79.20E 14KM.
MAY 10,1971 42.58N 71.29E 13KM.
OCT 28,1971 41.88N 72.35E 15KM
JUN 15,1971 41.39N 79.18E 96KM.
JUN 16,1971 41.49N 79.29E 14KM.
JAN 15,1972 40.17N 78.96E 8KM
APR 9,1972 42.09N 84.58E 21KM
JUN 2,1973 44.14N 83.60E 20KM
AUG 11,1974 39.34N 73.76E 7KM
AUG 11,1974 39.44N 73.67E 41KM
AUG 11,1974 39.46N 73.62E 26KM
AUG 27,1974 39.52N 73.82E 14KM

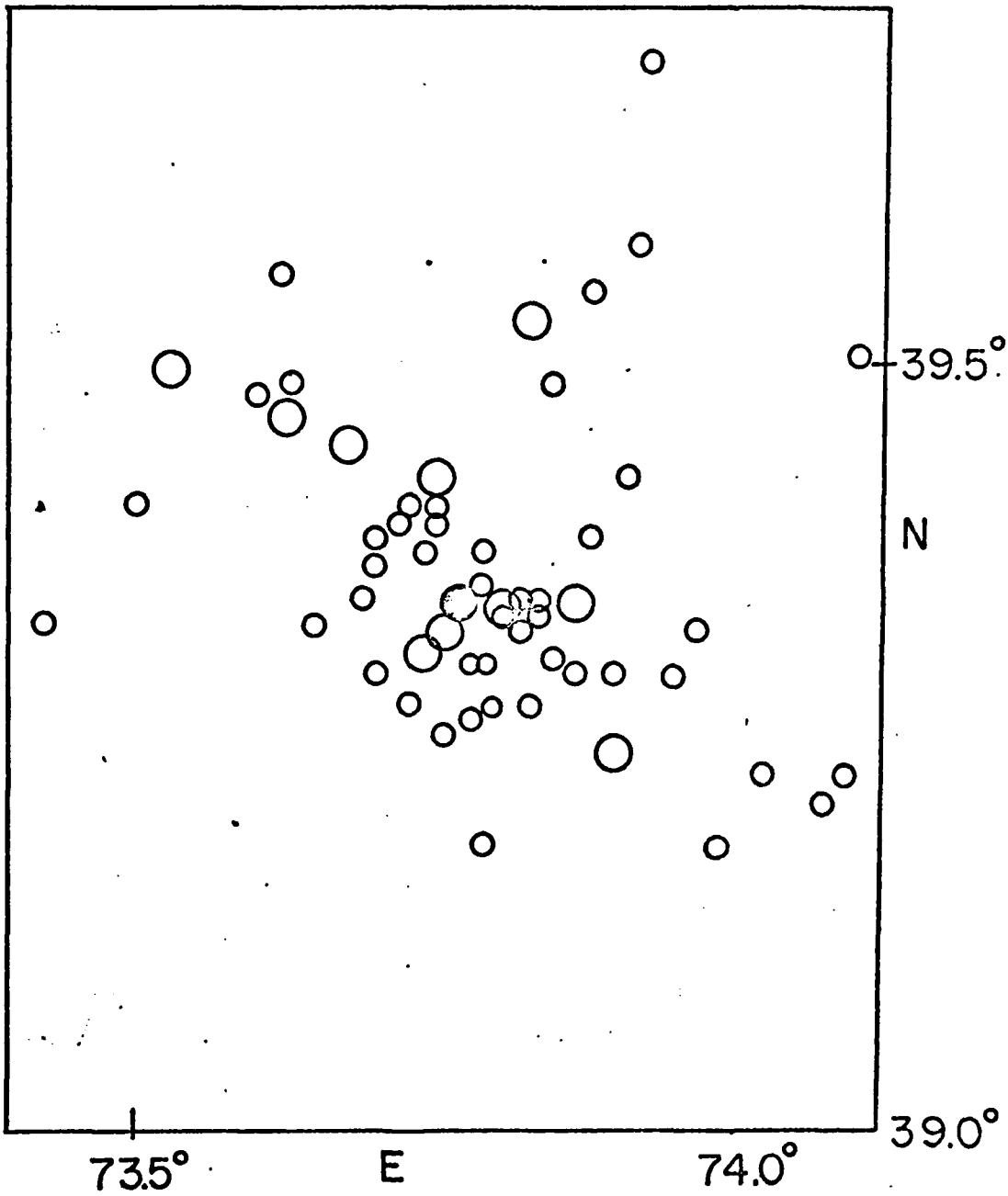

Fig. 4


IE073-00 IN039-30 IE073-30 E074-001
25NOV76 C N40-14/E074-06 N N40-14/E074-10 MSS 5 D SUN EL23 AZ150 191-9377-X-1-N-P-2L
IE073-00 E073-301 E074-001 N039-301
B
A
IE072-30 E073-001 N038-001 E073-301 E074-001
25NOV76 C N38-48/E073-37 N N38-49/E073-41 MSS 5 D SUN EL24 AZ149 191-9377-X-1-N-P-2L
IE072-30 E073-001 E073-301

Fig 5

Fig. 6